Energy momentum tensor, and the D-term of Q-balls

Manuel Mai and Peter Schweitzer

Energy momentum tensor, and the D-term of Q-balls

Manuel Mai[1] and Peter Schweitzer[2]

[1]*Department of Physics Yale University, New Haven, CT 06511-8499, U.S.A.*
[2] *Department of Physics, University of Connecticut, Storrs, CT 06269-3046, U.S.A.*
(Dated: September 2012)

We study the energy-momentum tensor of stable, meta-stable and unstable Q-balls in scalar field theories with U(1) symmetry. We calculate properties such as charge, mass, mean square radii and the constant d_1 ("D-term") as functions of the phase space angular velocity ω. We discuss the limits when ω approaches the boundaries of the region in which solutions exist, and derive analytical results for the quantities in these limits. The central result of this work is the rigorous proof that d_1 is strictly negative for all finite energy solutions in the Q-ball system.

I. INTRODUCTION

The matrix elements of energy momentum tensor $T_{\mu\nu}$ (EMT) [1] contain basic information, such as mass [2] and spin of the particle [3], and the constant d_1. This constant denotes the value of the corresponding form factor at zero-momentum transfer, and is the only experimentally unknown "charge" associated with the EMT. Its physical meaning was uncovered in [4] where it was shown that d_1 is related to the spatial distribution of internal forces. This is analog to the interpretation of the electric form factor as the Fourier transform of the electric charge distribution [5] (and subject to the same type of limitations [5, 6] due to relativistic corrections).

The EMT form factors can in principle be studied through generalized parton distribution functions [7, 8] accessible in hard exclusive reactions such as deeply virtual Compton scattering [9–12]. In this work we shall loosely refer to d_1 as the D-term, although both coincide strictly speaking only for asymptotically large renormalization scales [13]. Theoretical studies of EMT form factors were presented in chiral perturbation theory, lattice QCD, effective chiral field theories or models [13–23].

It is a striking observation that in all theoretical studies d_1 was found negative — for pions, nucleons, nuclei. Results from chiral soliton models [16–19] gave rise to the suspicion the sign of d_1 could be related to stability. The naturally emerging questions are: could the negative sign of d_1 be a model-independent feature, a theorem? And, is there really a relation between d_1 and stability?

This work is devoted to the study of the EMT of Q-balls [24, 25] with the aim to shed further light on these questions. Q-balls are non-topological solitons in theories with global Abelian [25] or non-Abelian [26] symmetries, and have been discussed in a variety of approaches with a wide range of applications in particle physics, cosmology, and astrophysics [27–46].

The Q-ball equations of motions admit stable, meta-stable and unstable solutions. This makes them an ideal ground for our purposes. In this work we will be interested in the ground state Q-ball solutions [25]. The equations of motions admit also radial excitations [37] which will be subject to a separate work [47].

The stability of Q-ball systems was studied in many works [37–42]. But this is, to the best of our knowledge, the first time this issue is addressed from the point of view of the EMT. In particular, we present the first rigorous proof in a dynamical system that d_1 must be negative. This supports the idea that the negative sign of d_1 could be a general feature. However, our results also show that there is no relation between the sign of d_1 and stability. The outline of this work is as follows.

In Sec. II, after a brief review of Q-balls, we derive the expressions for the energy density $T_{00}(r)$, pressure and shear forces, $p(r)$ and $s(r)$, related to the stress tensor $T_{ik}(r)$, and prove analytically that exact solutions of the Q-ball equations of motions satisfy the Laue condition $\int_0^\infty \mathrm{d}r\, r^2 p(r) = 0$ [48], which is a consequence of the conservation of the EMT, and which we show to be equivalent to the virial theorem [30]. This is analog to the situation in soliton models of the nucleon [16–18].

In Sec. III we study Q-ball properties such as charge, mass, mean square radii, and the D-term in a chosen potential as functions of the angular velocity ω in the U(1)-space in the region $\omega_{\min} < \omega < \omega_{\max}$ in which the equations of motion admit finite energy solutions. An interesting observation is that among the quantities we study d_1 varies most strongly with ω.

In Sec. IV and V we then focus on the behavior of the Q-ball properties as ω approaches the boundaries of the region in which finite energy solutions exist, i.e. the limits $\omega \to \omega_{\min}$ and $\omega \to \omega_{\max}$ respectively. We derive in both cases analytical results which describe the behavior the different quantities in these limits and which are fully supported by the numerical results.

In Sec. VI we formulate two independent proofs that d_1 is strictly negative for all solutions in the Q-ball system, and show that the sign of d_1 is not related to stability.

The Sec. VII contains a summary of our findings and the conclusions. Some technical details and supplementary results are discussed in the Appendix.

II. Q-BALLS

We consider the relativistic field theory [25] of a complex scalar field $\Phi(x)$ defined by the Lagrangian

$$\mathcal{L} = \frac{1}{2} \left(\partial_\mu \Phi^*\right)(\partial^\mu \Phi) - V \,. \qquad (1)$$

The potential $V \geq 0$ is defined in terms of the positive constants A, B, C (with $4AC > B^2$ to guarantee $V > 0$ for $\phi \neq 0$) as follows

$$V = A \left(\Phi^* \Phi\right) - B \left(\Phi^* \Phi\right)^2 + C \left(\Phi^* \Phi\right)^3 \,. \qquad (2)$$

The Lagrangian is invariant under global U(1) symmetry transformations $\Phi \to \Phi\, e^{i\alpha}$, $\Phi^* \to \Phi^*\, e^{-i\alpha}$ with α real. This system admits non-topological soliton solutions [25] which in the soliton rest frame are given by

$$\Phi(t, \vec{x}) = \exp(i\omega t)\, \phi(r) \,, \quad r = |\vec{x}| \,. \qquad (3)$$

The Euler-Lagrange equations of the theory in (1) imply for the radial field $\phi(r)$ the following differential equation (here and in the following primes denote differentiation with respect to the argument)

$$\phi''(r) + \frac{2}{r}\, \phi'(r) + \omega^2 \phi - V'(\phi) = 0 \,, \qquad (4)$$

which is subject to the boundary conditions

$$\phi(0) \equiv \phi_0 = \text{const}, \quad \phi'(0) = 0, $$
$$\phi(r) \to 0 \text{ for } r \to \infty \,. \qquad (5)$$

The Noether theorem applied to the global U(1) symmetry implies the conserved charge

$$Q = \int \mathrm{d}^3 x\, \rho_{\text{ch}}(r) \,, \quad \rho_{\text{ch}}(r) = \omega\, \phi(r)^2 \,. \qquad (6)$$

The sign of ω determines the sign of the charge Q. In the following we assume $\omega > 0$ without loss of generality. The presence of a continuous global symmetry is essential for the existence of the soliton. More precisely, finite energy solutions exist for ω in the range

$$\omega_{\min}^2 < \omega^2 < \omega_{\max}^2 \,, \qquad (7)$$

with

$$\omega_{\min}^2 = \min_\phi \left[\frac{2\, V(\phi)}{\phi^2}\right] = 2A\left(1 - \frac{B^2}{4AC}\right) > 0 \,,$$

$$\omega_{\max}^2 = V''(\phi)\Big|_{\phi=0} = 2A \,. \qquad (8)$$

From (4, 5) we obtain for $\phi(r)$ the following small- and large-r behavior (the dots indicate subleading terms)

$$\phi(r) = \phi_0 + \left(V'(\phi_0) - \omega^2 \phi_0\right)\frac{r^2}{6} + \dots \text{ small } r, \quad (9)$$

$$\phi(r) = \frac{c_\infty}{r} \exp\left(-r\sqrt{\omega_{\max}^2 - \omega^2}\right) + \dots \text{ large } r. \quad (10)$$

The constants ϕ_0 and c_∞ are known, of course, only after solving the boundary value problem (4, 5).

A. Stability criteria

Solutions for ω satisfying the existence condition (7) can be classified as (a) stable, (b) meta-stable, and (c) unstable Q-balls, see e.g. [42] for an overview.

(a) If M denotes the mass of the soliton, and m the mass of the field Φ, which is $m = \sqrt{2A} = \omega_{\max}$, then the absolute stability condition can be expressed as [29]

$$M < m\, Q \,, \quad m \equiv \omega_{\max} \,. \qquad (11)$$

(b) Meta-stable solutions do not satisfy (11) but are stable with respect to small fluctuations, and satisfy a weaker "classical stability condition" [24, 29] which can be formulated in the equivalent ways

$$\frac{\mathrm{d}}{\mathrm{d}\omega}\left(\frac{M}{Q}\right) \geq 0 \quad \Leftrightarrow \quad \frac{\mathrm{d}Q}{\mathrm{d}\omega} \leq 0 \quad \Leftrightarrow \quad \frac{\mathrm{d}^2 M}{\mathrm{d}Q^2} \leq 0 \,, \quad (12)$$

i.e. a critical ω_c (extreme charge Q_c) exists at which the slope (curvature) of the quantities in (12) changes.

(c) Solutions satisfying neither the stronger condition (11) nor the weaker condition (12) are unstable.

B. The EMT of Q-balls

For the theory defined by the Lagrangian (1) the canonical energy momentum tensor

$$T_{\mu\nu} = \frac{\partial \mathcal{L}}{\partial(\partial^\mu \Phi)}\, \partial_\nu \Phi + \frac{\partial \mathcal{L}}{\partial(\partial^\mu \Phi^*)}\, \partial_\nu \Phi^* - g_{\mu\nu}\, \mathcal{L} \qquad (13)$$

is symmetric and static. The energy density, which defines the mass $M = \int \mathrm{d}^3 x\, T_{00}$, is given by

$$T_{00}(r) = \frac{1}{2}\, \omega^2 \phi(r)^2 + \frac{1}{2}\, \phi'(r)^2 + V(\phi) \,. \qquad (14)$$

The T_{0k} components vanish, i.e. the Q-ball has spin zero. (Of course, Q-ball solutions can be assigned a non-zero spin by means of appropriate projection techniques [49].) Finally, the T_{ij} components describe the stress tensor

$$T_{ij} = \left(\frac{x_i x_j}{r^2} - \frac{1}{3}\, \delta_{ij}\right) s(r) + \delta_{ij}\, p(r) \qquad (15)$$

with the distribution of the shear forces, $s(r)$, and pressure, $p(r)$, given by

$$s(r) = \phi'(r)^2 \qquad (16)$$

$$p(r) = \frac{1}{2}\, \omega^2 \phi(r)^2 - \frac{1}{6}\, \phi'(r)^2 - V(\phi) \,. \qquad (17)$$

The dimensionless constant d_1 is defined through the stress tensor T_{ij} [4], and can be expressed in terms of $s(r)$ and $p(r)$ (cf. Sec. II C) as follows

$$d_1 = -\frac{4\pi}{3}\, M \int_0^\infty \mathrm{d}r\, r^4 s(r) \,, \qquad (18)$$

$$= 5\pi\, M \int_0^\infty \mathrm{d}r\, r^4 p(r) \,. \qquad (19)$$

The large-r asymptotics (10) ensures that all integrals (which define M, Q, d_1, mean square radii, etc) exist.

C. Consequences from conservation of EMT

For a static EMT $\partial^\mu T_{\mu\nu} = 0$ is equivalent to $\nabla^i T_{ij} = 0$ which, using the decomposition (15), implies [4]

$$\frac{2}{r} s(r) + \frac{2}{3} s'(r) + p'(r) = 0 \,. \tag{20}$$

In order to prove that (20) holds for Q-balls, we insert $s(r)$ and $p(r)$ from Eqs. (16, 17) into (20), which yields

$$\frac{2}{r} s(r) + \frac{2}{3} s'(r) + p'(r) \tag{21}$$
$$= \phi'(r) \left(\phi''(r) + \frac{2}{r} \phi'(r) + \omega^2 \phi(r) - V'(\phi) \right) = 0$$

due to the equations of motion in Eq. (4).

From (20) one can derive the equivalent representations (18, 19) for d_1 in terms of $s(r)$ and $p(r)$, and other general relations [16]. For instance, multiplying (20) by r^3 and integrating (by parts) over r from zero to infinity yields the "Laue condition" [48]

$$\int_0^\infty dr \, r^2 p(r) = 0 \,. \tag{22}$$

In order to prove (22) for Q-balls we integrate by parts (primes denote derivatives with respect to the arguments, the finite upper integration limit R is for later purposes)

$$\int_0^R dr \, r^2 \, p(r) = \left[\frac{r^3}{3} p(r) \right]_0^R - \int_0^R dr \, \frac{r^3}{3} \, p'(r) \tag{23}$$

Next we notice that

$$p'(r) = \left(-\frac{1}{3} \phi''(r) + \omega^2 \phi(r) - V'(\phi) \right) \phi'(r)$$
$$= -\frac{4}{3} \phi'(r) \phi''(r) - \frac{2}{r} \phi'(r)^2$$
$$= -\frac{2}{3r^3} \left[r^3 \phi'(r)^2 \right]' \tag{24}$$

where we used $\omega^2 \phi - V'(\phi) = -\phi''(r) - \frac{2}{r} \phi'(r)$ in the first step which holds due to the equations of motion (4). Hence, using $s(r) = \phi'(r)^2$, we obtain

$$\int_0^R dr \, r^2 p(r) = \left[\frac{r^3}{3} \left(p(r) + \frac{2}{3} s(r) \right) \right]_0^R \,. \tag{25}$$

The small- and large-r behavior of the solutions in (9) guarantees that the lower and (after taking $R \to \infty$) upper integration limits in (25) vanish which proves (22).

It is instructive to prove (22) independently as follows. Let $\phi(r)$ be a Q-ball solution with charge Q and mass M, which we rewrite by means of (6, 14) in terms of the "charge," "surface," and "potential energies" (where we leave the number of dimensions $D = 3$ general)

$$M = \frac{1}{2} E_{\text{ch}} + \frac{1}{2} E_{\text{surf}} + E_{\text{pot}} \tag{26}$$

$$E_{\text{surf}} = \int d^D x \, \phi'(r)^2 \,, \quad E_{\text{pot}} = \int d^D x \, V(\phi) \,,$$

$$I = \int d^D x \, \phi(r)^2 \,, \quad E_{\text{ch}} = \frac{Q^2}{I} \,. \tag{27}$$

We consider dilatational variations $\phi(r) \to \phi(\lambda r)$ of the solutions with a positive parameter λ. Substituting in the integrals in (27) $\vec{x} \to \lambda \vec{x}$ yields

$$M(\lambda) = \frac{1}{2} E_{\text{ch}} \lambda^D + \frac{1}{2} E_{\text{surf}} \lambda^{2-D} + E_{\text{pot}} \lambda^{-D} \,. \tag{28}$$

$M'(\lambda) = 0$ and $M''(\lambda) > 0$ at $\lambda = 1$, because $\phi(\lambda r)$ for $\lambda = 1$ is a solution which minimizes the energy functional. We obtain, using again (6) and the definitions in (27),

$$0 \overset{!}{=} \frac{1}{D} \frac{\partial M(\lambda)}{\partial \lambda} \bigg|_{\lambda=1} = \frac{1}{2} E_{\text{ch}} + \frac{2-D}{2D} E_{\text{surf}} - E_{\text{pot}}$$
$$= \int d^D x \left\{ \frac{1}{2} \omega^2 \phi(r)^2 - \frac{D-2}{2D} \phi'(r)^2 - V(\phi) \right\}. \tag{29}$$

For $D = 3$ we identify the expression (17) for $p(r)$ in the curly brackets of (29) which completes our alternative proof of (22). Eq. (29) is known as virial theorem [30]. Notice that (29) can be used to eliminate, for instance, the potential energy term from (26), leading to

$$M = \omega Q + \frac{1}{D} E_{\text{surf}} \,. \tag{30}$$

As a last application of (20) we integrate this equation over r from zero to infinity. This yields the relation [16]

$$p(0) = 2 \int_0^\infty dr \, \frac{s(r)}{r} \,, \tag{31}$$

which provides a helpful cross check for numerical calculations, and implies the following interesting relation: inserting in (31) the expressions (16, 17) yields

$$\frac{1}{2} \omega^2 \phi_0^2 - V(\phi_0) = 2 \int_0^\infty dr \, \frac{\phi'(r)^2}{r} \,. \tag{32}$$

This is interesting, because the left-hand-side depends on ϕ_0 only while the right-hand-side is a functional of $\phi'(r)$ where ϕ_0 drops out. Below in Sec. III A we will discuss the physical interpretation of (32).

D. Relations among Q-ball properties

Further interesting relations among different Q-ball properties follow from combining (6, 14, 16, 17) as

$$T_{00}(r) + p(r) = \omega \rho_{\text{ch}}(r) + \frac{1}{3} s(r) \,. \tag{33}$$

Integrating (33) over d^3x we recover (30) for $D = 3$ (the derivations are equivalent, but (30) elucidates the relation of the factor $\frac{1}{3}$ to the dimensionality of the space). Next, we define the "surface tension" γ and the mean square radius $\langle r_s^2 \rangle$ of the shear forces $s(r)$ as follows

$$\gamma = \int\limits_0^\infty \mathrm{d}r\, s(r)\,, \quad \langle r_s^2 \rangle = \frac{\int\limits_0^\infty \mathrm{d}r\, r^2 s(r)}{\int\limits_0^\infty \mathrm{d}r\, s(r)}\,. \tag{34}$$

Thus, the surface energy $E_{\mathrm{surf}} = \int \mathrm{d}^3x\, s(r)$, Eq. (27), can be written as $E_{\mathrm{surf}} = 4\pi \langle r_s^2 \rangle \gamma$ which is what one expects for a spherical object with a well-defined surface and radius $\langle r_s^2 \rangle^{1/2}$. In Sec. IV we will see that these notions make sense for Q-balls in a certain limit.

Finally, we weight (33) with r^2, and integrate over d^3x. This allows to express d_1 in terms of other properties as

$$d_1 = \frac{5}{9}\left(\omega\, Q\, M\, \langle r_Q^2 \rangle - M^2\, \langle r_E^2 \rangle\right), \tag{35}$$

with the mean square radii of energy and charge densities defined as

$$\langle r_E^2 \rangle = \frac{\int \mathrm{d}^3x\, r^2\, T_{00}(r)}{\int \mathrm{d}^3x\, T_{00}(r)}\,, \quad \langle r_Q^2 \rangle = \frac{\int \mathrm{d}^3x\, r^2\, \rho_{\mathrm{ch}}(r)}{\int \mathrm{d}^3x\, \rho_{\mathrm{ch}}(r)}\,. \tag{36}$$

E. Parameters and numerics

In our numerical study we fix the parameters as

$$A = 1.1\,, \quad B = 2.0\,, \quad C = 1.0\,. \tag{37}$$

(for which in [37] radial Q-ball excitations were found; the latter originally motivated our study, but will be discussed in a separate work [47]). This yields the following range of allowed ω-values

$$0.2 < \omega^2 < 2.2\,. \tag{38}$$

The parameter set (A, B, C) could be assigned physical units, say $(\mathrm{GeV}^2, \mathrm{GeV}^0, \mathrm{GeV}^{-2})$. Then ω, M would be given in GeV, mean square radii in GeV^{-2}, etc. But for simplicity we will work with dimensionless quantities.

The numerical method is as follows. For a given ω the differential equation (4) is solved with slightly shifted initial conditions $\phi(\varepsilon) \equiv \phi_\varepsilon$ and $\phi'(\varepsilon) = \frac{1}{3}(V'(\phi_\varepsilon) - \omega^2\phi_\varepsilon)\varepsilon$ with numerical parameters ε in the range 10^{-10} to 10^{-4}. We checked that the results do not depend on ε. Finite energy solution are found using the shooting method by varying the initial value ϕ_ε until $\phi(r) \to 0$ at large r.

The quality of the numerics is monitored by testing that (i) the differential equation (20) holds, (ii) the Laue condition (22) is valid, (iii) different expressions for d_1 in (18, 19, 35) yield the same result, (iv) the same value for $p(0)$ follows from (17, 31). We find a relative numerical accuracy of $\mathcal{O}(10^{-6})$ or better.

III. GROUND STATE Q-BALLS

In this Section we discuss the ground state properties of Q-balls in our potential (2) for different values of ω.

A. Effective potential U_{eff} and ϕ_0

Identifying $r \to t$ and $\phi(r) \to x(t)$, the equation of motion (4) can be read [25] as the Newtonian equation

$$\ddot{x}(t) = F_{\mathrm{fric}} - \nabla U_{\mathrm{eff}}(x) \tag{39}$$

$$F_{\mathrm{fric}} = -\frac{2}{t}\,\dot{x}(t)\,, \quad U_{\mathrm{eff}} = \frac{1}{2}\omega^2\, x^2 - V(x)\,.$$

describing the motion of a particle of unit mass under the influence of the time- and velocity-dependent friction F_{fric} in the effective potential U_{eff} shown in Fig. 1. The initial and boundary values (5) mean that at $t = 0$ the particle starts from the position x_0 with zero velocity, and comes to rest in the origin $x = 0$ after infinite time. Thus $x(t) > 0$ and the particle never stops at finite t. This implies decreasing monotony of the ground state fields, $\phi(r) > 0$ and $\phi'(r) < 0$ for $0 < r < \infty$.

The pressure (17) is given at $r = 0$ by $p(0) = U_{\mathrm{eff}}(\phi_0)$ and the condition (7) guarantees the existence of a region of ϕ with $U_{\mathrm{eff}}(\phi) > 0$ [25]. This proves that

$$p(0) > 0\,. \tag{40}$$

Now also the physical interpretation of (32) is evident. The left hand side of (32) is the initial potential energy. The right hand side of (32) is the work $W = \int F_{\mathrm{fric}}\mathrm{d}x$ the particle does to overcome the friction before coming to rest at $x = 0$ with zero effective potential energy.
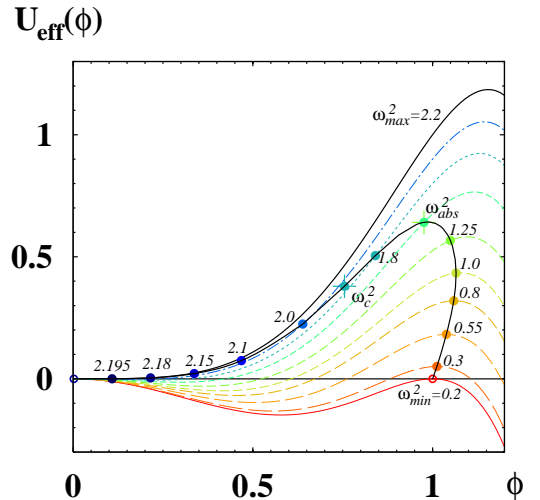

FIG. 1: The effective potentials $U_{\mathrm{eff}}(\phi) = \frac{1}{2}\omega^2\phi^2 - V(\phi)$ as functions of ϕ for selected values of ω^2 in the range (38). The circles show the initial values ϕ_0 for each ω^2, which lie on a curve starting and ending at the limiting values $\omega_{\mathrm{min}}^2 = 0.2$ and $\omega_{\mathrm{max}}^2 = 2.2$ (marked by open circles). The special values $\omega_c^2 \approx 1.9$ and $\omega_{\mathrm{abs}}^2 \approx 1.55$ are discussed in text.

Solutions exist for all ω in the range $\omega_{\min} < \omega < \omega_{\max}$. With our numerical method, we were able to find solutions in the subinterval $0.216 \leq \omega^2 \leq 2.195$.

The effective potentials $U_{\text{eff}}(\phi) = \frac{1}{2}\omega^2\phi^2 - V(\phi)$ are shown in Fig. 1 for selected ω including the limiting cases $\omega_{\min}$ and $\omega_{\max}$. On each of the $U_{\text{eff}}(\phi)$-curves in Fig. 1 we marked the initial conditions ϕ_0 which solve the boundary value problem (4, 5). The $U_{\text{eff}}(\phi_0)$ for different ω lie on a curve which exhibits a global maximum close to $\omega_{\text{abs}}^2 \approx 1.55$, and changes the curvature around $\omega_c^2 \approx 1.9$ (these frequencies will be discussed in detail in Sec. III C). This curve starts and ends at the limiting points

$$\lim_{\omega \to \omega_{\max}} \phi_0 = 0\,, \qquad \lim_{\omega \to \omega_{\min}} \phi_0 = \sqrt{\frac{B}{2C}} = 1\,, \qquad (41)$$

with the potential $U_{\text{eff}}(\phi_0) \to 0$ in both cases, see App. A. $U_{\text{eff}}(\phi_0)$ as function of ϕ_0 is not unique for $\phi_0 \geq 1$.

B. Solutions $\phi(r)$ and densities

In this section we describe the results for $\phi(r)$ and the various densities. Some of our observations concerning the behavior of the densities in the limits $\omega \to \omega_{\min,\max}$ will be made more rigorous in Secs. IV and V.

The ground state solutions $\phi(r)$, which are uniquely determined in terms of the initial values ϕ_0 discussed in the previous section, are shown in Fig. 2a as functions of r for selected values of ω in the range $0.216 \leq \omega^2 \leq 2.195$ our numerics can handle. We have chosen a logarithmic r-scale to better show the features of all solutions in a single plot. On a logarithmic scale the $\phi(r)$ are nearly constant for $r < 0.1$, and have the small-r behavior (9). Their large-r asymptotics agrees with (10).

With decreasing ω the solutions $\phi(r)$ remain nearly constant at their initial values in a region $0 \leq r < R_0$ and form increasingly long plateaus from which they then drop down to their large-r asymptotics (10) over decreasingly narrow transition regions with thicknesses $\ll R_0$. Here R_0 can be understood as the "size" of the Q-ball, which will be defined below more accurately. In the limit $\omega \to \omega_{\min}$ the field $\phi(r) \to \phi_0\,\Theta(R_0 - r)$ where $R_0 \to \infty$ and $\phi_0 \to 1$, see (41) and App. A. This behavior ("thin-wall limit") can be strictly derived [25]. In the opposite limit, as ω increases, the solutions $\phi(r)$ become more wide-spread and their magnitude decreases, see (41) and App. A.

Fig. 2b shows the charge densities $\rho_{\text{ch}}(r) = \omega\phi(r)^2$ as functions of r. Also the charge densities exhibit for small ω extended plateaus in the region $0 \leq r \lesssim R_0$ inside the Q-balls, and drop abruptly to zero outside. For $\omega \to \omega_{\max}$ the charge densities become more wide-spread and their magnitudes show an overall decrease.

Fig. 2c shows the energy densities $T_{00}(r)$, which look qualitatively similar to charge densities for $\omega \gtrsim 1$. But for $\omega \lesssim 1$ the energy densities start to develop a "bump" around R_0, and as ω approaches $\omega_{\min}$ the bump becomes
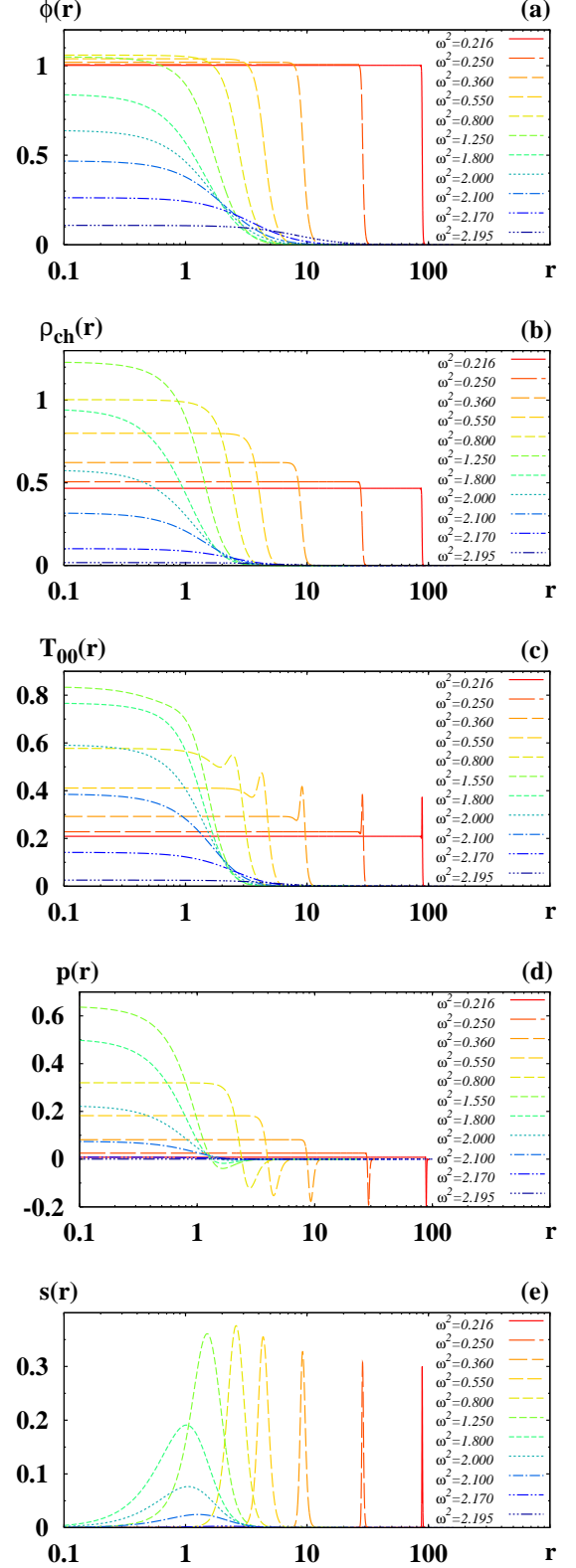

FIG. 2: Field $\phi(r)$, charge density $\rho_{\text{ch}}(r)$, energy density $T_{00}(r)$, pressure $p(r)$, shear force distribution $s(r)$ vs. r for Q-ball ground state solutions for selected values of ω.

a characteristic "spike." The reason for that is that for $\omega \gtrsim 1$ the Q-balls are "diffuse" objects, while for $\omega \lesssim 1$ they start to develop a more and more well-defined "edge." In fact, as $\omega \to \omega_{\min}$ the notions of a "surface" and "surface tension" become better defined [25]. The characteristic bump/spike structure in $T_{00}(r)$ at $r \sim R_0$ reflects the contribution of the surface energy. In the limit $\omega \to \omega_{\max}$ we find $T_{00}(r) \to 0$. In the limit $\omega \to \omega_{\min}$ we have $T_{00}(r) \to$ const for $0 \le r < R_0$ with a surface energy contribution proportional to $\delta(r-R_0)$ with $R_0 \to \infty$.

Fig. 2d shows the pressures $p(r)$ as functions of r. For all ground state solutions the pressures are positive "inside" and "negative" outside in agreement with general expectations (79). We are now in the position to provide an exact definition of the scale R_0 as the point where the pressure vanishes, i.e. $p(R_0) = 0$ with $0 < R_0 < \infty$. The Laue condition is fulfilled because the integrals $\int_0^{R_0} dr\, r^2 p(r)$ and $\int_{R_0}^{\infty} dr\, r^2 p(r)$ have opposite signs and precisely cancel. Numerically the sum of these 2 contributions normalized with respect to the sum of their moduli is of $\mathcal{O}(10^{-6})$ or smaller. In the limit $\omega \to \omega_{\max}$ we find $p(r) \to 0$. For $\omega \to \omega_{\min}$ we obtain $p(r) \to$ const for $0 \le r < R_0$ with a surface energy contribution proportional to $-\delta(r-R_0)$ and a diverging Q-ball size R_0.

Fig. 2e shows the shear forces $s(r)$ which are best suited to discuss the concepts of "diffuseness" or "edge". From (9, 10) we see $s(r) \to 0$ as $r \to 0$ or $r \to \infty$, and from Eq. (16) we see it is an evidently positive quantity, i.e. $s(r)$ must have a global maximum somewhere. To determine the position of this maximum consider $s'(r) = 2\phi'(r)\phi''(r)$. Now due to the monotony property of $\phi(r)$ discussed in Sec. III A, we have $\phi'(r) = 0$ only at $r = 0$ and at infinity. I.e. the maximum of $s(r)$ coincides with the point where $\phi''(r) = 0$. This change of curvature occurs in the vicinity of the "edge" of the Q-ball, and in the limit $\omega \to \omega_{\min}$ precisely at $r = R_0$ where $s(r)$ becomes proportional to a $\delta(r - R_0)$ with a coefficient related to the surface tension. As ω approaches $\omega_{\max}$ the shear force distribution becomes wider and wider, which indicates a more and more diffuse "edge" of the Q-ball.

C. ω_c and ω_{abs}

The frequencies ω_c and ω_{abs} were discussed in the sequence of Eq. (12), and mentioned in the context of Fig. 1. In this Section we discuss how they appear in the numerical results. At the frequency $\omega = \omega_c \approx 1.38$

1. $(M/Q)(\omega)$ has a global maximum, Fig. 3a,

2. $Q(\omega)$ has a global minimum, Fig. 3b,

3. $M(Q)$ has a branch point at $Q_c = Q(\omega_c)$, Fig. 3c.

The frequency ω_c and charge Q_c define classical stability. For $\omega < \omega_c$ we have $(M/Q)'(\omega) > 0$, and $Q'(\omega) < 0$.
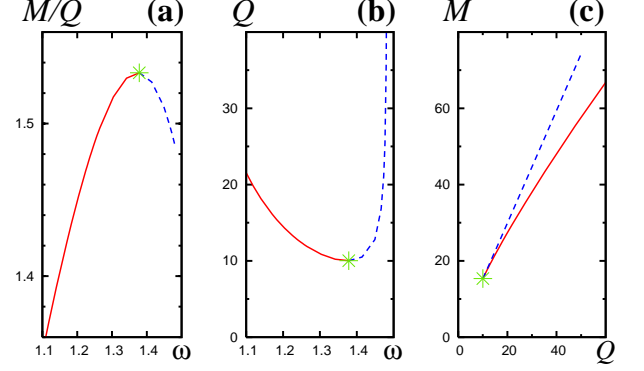

FIG. 3: **(a)** M/Q as function of ω, with $(M/Q)'(\omega) > 0$ in the range $\omega < \omega_c \approx 1.38$ (solid line). **(b)** Q as function of ω, with $Q'(\omega) < 0$ for $\omega < \omega_c$ (solid line). **(c)** M vs. Q, with $M''(Q) < 0$ in the branch denoted by the solid line. The solid (dotted) lines correspond to the region of classically stable (unstable) Q-balls, see Eq. (12).
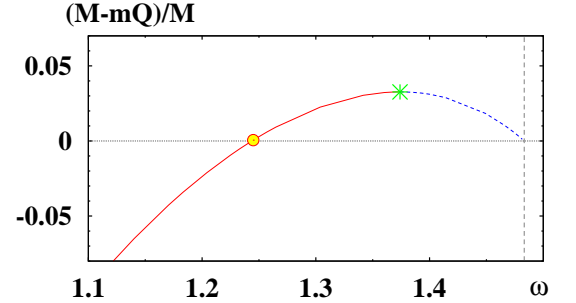

FIG. 4: $(M - mQ)/M$ as function of ω which exhibits a maximum at ω_c. For $\omega < \omega_{\mathrm{abs}}$ we have $M - mQ < 0$ and the Q-balls are absolutely stable. For $\omega_{\mathrm{abs}} < \omega < \omega_c$ the Q-balls are meta-stable, and for $\omega_c < \omega < \omega_{\max}$ they are unstable. $(M - mQ)$ approaches zero as $\omega \to \omega_{\max}$ which is indicated by the vertical line.

For $Q > Q_c$ we have $M''(Q) < 0$. These are equivalent criteria for the stability of Q-balls against small fluctuations. In Fig. 3 the branches of classically stable Q-balls are shown as solid lines, while the unstable branches are depicted as dotted lines.

Classical stability is a necessary but not sufficient condition for stability. For a Q-ball to be absolutely stable it is required $M < mQ$, see Eq. (11). Fig. 4 shows $M - mQ$ normalized with respect to M as function of ω. The quantity $(M - mQ)/M$ is negative for $\omega < \omega_{\mathrm{abs}} \approx 1.245$ (and has a global maximum at $\omega = \omega_c$ which follows from the fact that $M(\omega)$ and $Q(\omega)$ have extrema there). Thus, for $\omega < \omega_{\mathrm{abs}}$ the Q-balls are absolutely stable. In the region $\omega_{\mathrm{abs}} < \omega < \omega_c$ they are meta-stable. For $\omega > \omega_c$ we have unstable Q-balls.

In the limit $\omega \to \omega_{\max} \equiv m$ one observes $M \to mQ$, see Fig. 4. This means the unstable Q-balls dissociate into Q-clouds, i.e. into a gas of free quanta [28].
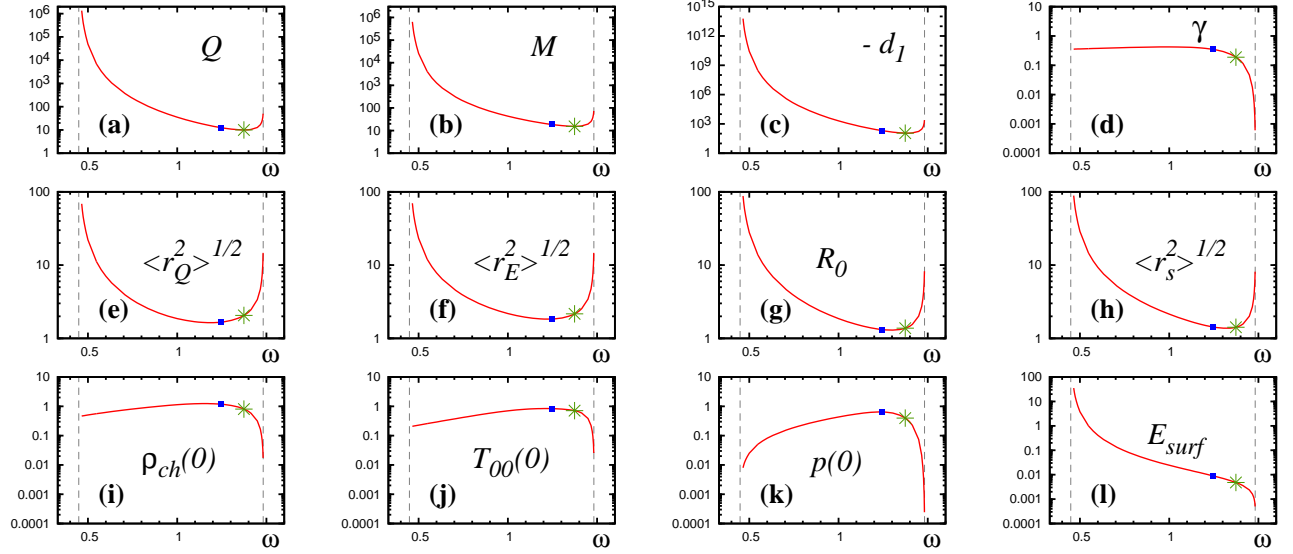
FIG. 5: Ground state properties of Q-balls as functions of ω. (a) charge Q, Eq. (6). (b) mass M, defined before Eq. (14). (c) constant d_1, Eq. (18). (d) "surface tension" γ, Eq. (34). The mean square radii of (e) charge and (f) energy densities, Eq. (36), and (h) shear forces, Eq. (34). (g) position R_0 of the zero of the pressure. The values of densities in the centers of Q-balls for (i) charge density, (j) energy density, (k) pressure, Eqs. (6, 14, 17). (l) The "surface energy" defined in (27). The special value $\omega_{\mathrm{abs}} \approx 1.245$ ($\omega_c \approx 1.38$) is marked by a square (star). The vertical lines indicate the limits $\omega_{\min} \approx 0.447$ and $\omega_{\max} \approx 1.483$.

D. Ground state properties

In this Section we study "global" Q-ball properties, appropriate integrals of the "local" densities from Sec. III B. The numerical results are shown in Fig. 5 which is organized as follows. The columns show as functions of ω quantities associated with (from left to right) the distributions of charge, energy, pressure and shear forces. Values of ω_{abs}, ω_c, $\omega_{\min/\max}$ are indicated in all plots.

Figs. 5a–d show Q, M, d_1, γ. At $\omega = \omega_c$ charge $Q(\omega)$ and mass $M(\omega)$ exhibit global minima, see (12), while in the vicinity of $\omega \approx \omega_c$ the "surface tension" $\gamma(\omega)$ exhibits the largest curvature, and $-d_1(\omega)$ a global minimum.

Figs. 5e–h show the different length scales of Q-balls: square roots of the mean square radii of the charge and energy densities and shear forces, Eqs. (34, 36), and R_0 which is where $p(r)$ changes sign. The behavior is qualitatively similar: all radii increase as $\omega \to \omega_{\min/\max}$, and have global minima around $\omega \approx \omega_{\mathrm{abs}}$ (for the minimum of $\langle r_s^2 \rangle^{1/2}$ we cannot exclude that it is, within numerical accuracy, exactly at ω_{abs}).

Figs. 5i–k shows the charge density, energy density, and pressure at the center of the Q-balls as functions of ω. These quantities exhibit maxima around ω_{abs}.

Since $s(0)$ vanishes, it would make no sense to show this quantity in analogy with Figs. 5i–k. Instead, in Fig. 5l we show the "surface energy," Eq. (27), as function of ω. As ω increases from $\omega_{\min}$ to $\omega_{\max}$ the surface energy decreases monotonically, which is compatible with the view that with increasing ω the Q-ball becomes a more and more diffuse object, see Sec. III B, such that the role of a "surface energy" become less and less impor-

tant. $E_{\mathrm{surf}}(\omega)$ changes the curvature at the point $\omega = \omega_c$ within numerical accuracy.

Some of the quantities vary strongly with ω, for instance d_1 extends over 12 orders of magnitude. This is not surprising since we compare Q-balls with different masses and sizes. For each quantity one could find "natural units" in order to make (from this point of view) the comparisons quantitatively more meaningful. The dimensionless constant d_1 has the natural units $(\mathrm{mass} \times \mathrm{length})^2$. To see this notice that it can be obtained from $d_1 = \frac{1}{3} M \int d^3 x \, r^2 s(r)$, and $\int d^3 x \, s(r)$ has dimension mass, since $s(r)$ and $T_{00}(r)$ have the same dimensions. Thus, one choice of "natural units" to measure d_1 could be $M^2 \langle r_i^2 \rangle$ with $i = s, E$. In Fig. 6 we see that in these units the constant d_1 varies much more moderately. In fact, for Q-balls of all ω we find that $0 < (-d_1)/(M^2 \langle r_s^2 \rangle) < 0.3$ holds.
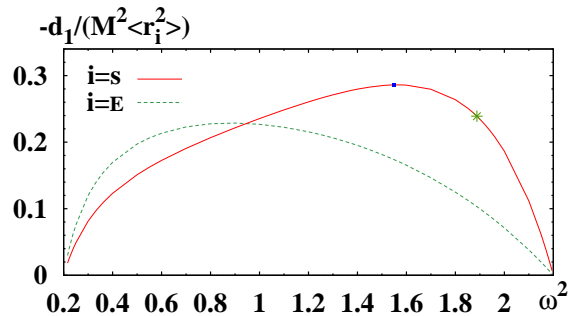

FIG. 6: $(-d_1)$ in units of $M^2 \langle r_i^2 \rangle$ ($i = s, E$) as function of ω^2. These units take into account the true dimensionality of d_1.

IV. THE LIMIT $\omega \to \omega_{\min}$

In this section we discuss Q-ball properties in the limit $\omega \to \omega_{\min}$, the so-called "thin wall" limit. In this limit the solutions describe objects of increasing size R with uniform charge distribution for $r < R$, which drops to zero over a narrow transition region ("thin wall") [25]. In some sense the Q-balls resemble liquid drops.

In a liquid drop of the size R the pressure distribution is $p(r) = p_0 \Theta(R - r) - \frac{1}{3} p_0 R \delta(R - r)$ where p_0 denotes the constant pressure inside the drop. This $p(r)$ satisfies the Laue condition (22). The shear forces are given by $s(r) = \gamma \delta(R - r)$, and the differential equation (20) leads to the Young-Laplace relation $\gamma = \frac{1}{2} p_0 R$ [50].

In the following we will "test" the predictions from the liquid drop picture using our numerical results, and derive analytically relations valid in the limit $\omega \to \omega_{\min}$.

In Fig. 2 we have seen that the solutions and densities approach the expected liquid drop shapes, see Sec. III B. Let us highlight here the shear force distribution. Fig. 7 shows $s(r) R_0 / \gamma$ as function of r/R_0 in the "edge region" for selected ω close to $\omega_{\min}$. The curves are scaled such that the areas under the graphs are normalized to unity. Clearly, as ω approaches $\omega_{\min}$ the shear force distributions peak more and more strongly in a narrow region concentrated around $r/R_0 \approx 1$. The "edge region" makes makes 5% and less of the size of the Q-ball, as expected.

That the Q-ball size diverges as $\omega \to \omega_{\min}$ is apparent from Figs. 5e–h. Our first quantitative expectation is that both the radius R_0 describing the position of the zero of the pressure and $\langle r_s^2 \rangle^{1/2}$ characterize equally well the position of the "edge" of the Q-ball. Hence we expect
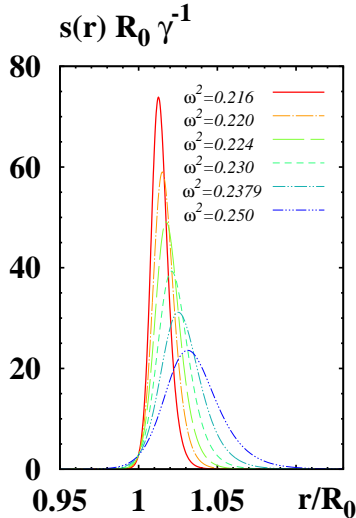
these radii to coincide for $\omega \to \omega_{\min}$, i.e.

$$\lim_{\omega \to \omega_{\min}} \frac{\langle r_s^2 \rangle}{R_0^2} = 1 \,. \tag{42}$$

The numerical results in Fig. 8a support Eq. (42).

In the following we choose $\langle r_s^2 \rangle^{1/2}$ as a reference length scale for the size of the Q-ball in the liquid drop limit, and define the "surface" and "volume" of a Q-ball as

$$A_s = 4\pi \langle r_s^2 \rangle \,, \quad V_s = \frac{4\pi}{3} \langle r_s^2 \rangle^{3/2} \,. \tag{43}$$

The charge distribution becomes $\rho_{\mathrm{ch}}(r) = \rho_0 \Theta(R - r)$ in the liquid drop limit, yielding $\langle r_{\mathrm{ch}}^2 \rangle = \frac{3}{5} R^2$ for the mean square charge radius in Eq. (36). The situation is analog for $\langle r_E^2 \rangle$, although $T_{00}(r)$ has a δ-function-type "spike" at $r = R$ due to surface energy, as can be seen in Fig. 2c.
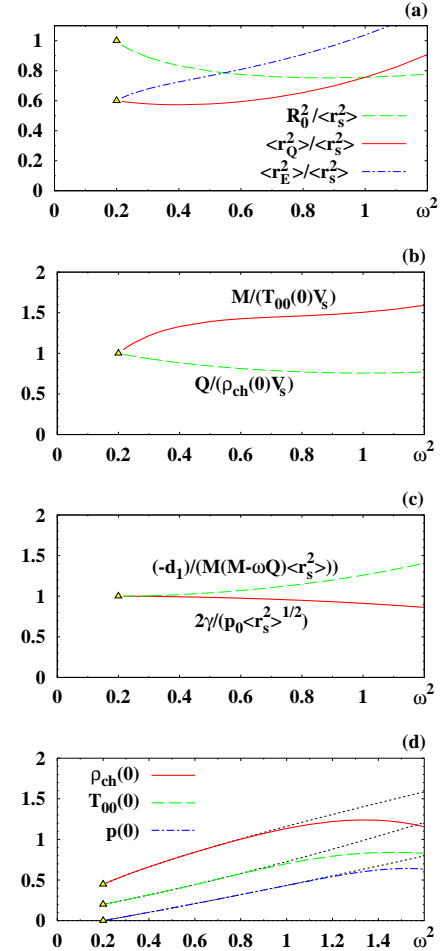

FIG. 8: Q-ball properties as functions of ω^2 in the limit $\omega \to \omega_{\min}$. (a) the ratios $R_0^2/\langle r_s^2 \rangle$, $\langle r_Q^2 \rangle/\langle r_s^2 \rangle$, $\langle r_E^2 \rangle/\langle r_s^2 \rangle$. (b) $M/(T_{00}(0)V_s)$ and $Q/(\rho_{\mathrm{ch}}(0)V_s)$. (c) $2\gamma/(p(0)\langle r_s^2 \rangle^{1/2})$ and $(-d_1)/(M(M-\omega Q)\langle r_s^2 \rangle)$. (d) $\rho_{\mathrm{ch}}(0)$, $T_{00}(0)$, $p(0)$. The solid, dashed, dashed-dotted lines show our numerical results, which approach the predicted limits marked by symbols. In Fig. 8d the thin lines are the analytic results derived from Eq. (50).

FIG. 7: $s(r) R_0 / \gamma$ as function of r/R_0 in the "edge region," for selected values of ω in the range $0.216 \leq \omega^2 \leq 0.25$. The curves are scaled such that the areas under the graphs are normalized to unity. The figure shows that with ω^2 approaching $\omega_{\min}^2 = 0.2$ the shear forces approach their liquid drop limit $s(r) = \gamma \delta(r - R_0)$ where γ denotes the surface tension, and R_0 the position at which the pressure vanishes.

But the surface energy is proportional to R^2, while the contribution of the constant bulk matter density inside the drop is proportional to R^3, so the influence of the spike can be neglected for a large drop. Hence, we expect

$$\lim_{\omega \to \omega_{\min}} \frac{\langle r_{\mathrm{ch}}^2 \rangle}{\langle r_s^2 \rangle} = \frac{3}{5}, \quad \lim_{\omega \to \omega_{\min}} \frac{\langle r_E^2 \rangle}{\langle r_s^2 \rangle} = \frac{3}{5}, \qquad (44)$$

and the numerical results in Fig. 8a support this. For the above discussed reasons we can furthermore expect

$$\lim_{\omega \to \omega_{\min}} \frac{M}{T_{00}(0)\,V_s} = 1\,,$$
$$\lim_{\omega \to \omega_{\min}} \frac{Q}{\rho_{\mathrm{ch}}(0)\,V_s} = 1\,. \qquad (45)$$

which is also confirmed, see Fig. 8b.

Surface and surface tension γ are abstract notions for arbitrary Q-balls which are *defined* through Eq. (34). One way to check the usefulness of those definitions provides the Young-Laplace relation, which implies

$$\lim_{\omega \to \omega_{\min}} \frac{2\gamma}{p_0 \langle r_s^2 \rangle^{1/2}} = 1\,. \qquad (46)$$

Notice that because of our definitions (34, 43) and (30), we always have the relation

$$\frac{2\gamma}{p_0 \langle r_s^2 \rangle^{1/2}} = \frac{2(M - \omega Q)}{p_0 V_s}\,. \qquad (47)$$

From (19) we obtain for a liquid drop $d_1^{\mathrm{drop}} = -\frac{4\pi}{3} M\gamma R^4$. Inserting here the expression for γ from (47) yields

$$\lim_{\omega \to \omega_{\min}} \frac{(-1)d_1}{M(M - \omega Q)\langle r_s^2 \rangle} = 1\,. \qquad (48)$$

Fig. 8c confirms both relations (46) and (48).

Next let us focus on the center properties of Q-balls. For $\omega \to \omega_{\min}$ the limiting value of the field $\phi(r)$ at $r = 0$ assumes the value $\phi_{\mathrm{const}}^2 = B/(2C)$, see (41) and App. A. For our potential and choice of parameters this means

$$\lim_{\omega \to \omega_{\min}} \rho_{\mathrm{ch}}(0) = \omega_{\min} \phi_{\mathrm{const}}^2 = \sqrt{0.2},$$
$$\lim_{\omega \to \omega_{\min}} T_{00}(0) = \omega_{\min}^2 \phi_{\mathrm{const}}^2 = 0.2\,,$$
$$\lim_{\omega \to \omega_{\min}} p(0) = 0\,, \qquad (49)$$

which is supported by our results in Fig. 8d. The result for $p(0)$ is derived alternatively in App. B.

We can go a step further and derive predictions from the liquid drop picture for the densities in (49) also for $\omega \neq \omega_{\min}$. This can be done because the probably most important features for $\omega > \omega_{\min}$ are the finite size of the Q-ball, and its diffuse "edge." But these features become important "far away" from the Q-ball center. So one would expect the liquid drop approach to give useful approximations for $\rho_{\mathrm{ch}}(0)$, $T_{00}(0)$, and $p(0)$ not only for $\omega = \omega_{\min}$ but also for ω in some vicinity of $\omega_{\min}$.

The result for $\phi_{\mathrm{const}}(\omega)$ follows from Eq. (A2) using the plus sign, and can be written as

$$\phi_{\mathrm{const}}^2(\omega) = \frac{B}{C}\left(\frac{1}{3} + \frac{1}{6}\sqrt{1 + \frac{6C}{B^2}(\omega^2 - \omega_{\min}^2)}\right). \qquad (50)$$

Fig. 8d shows that (50) provides excellent approximations for the exact ω-dependencies of $\rho_{\mathrm{ch}}(0)$, $T_{00}(0)$, $p(0)$ from up to $\omega^2 \lesssim 1$. The reason for that can be seen in Fig. 1. In our potential, the "particles" (in the "particle motion" picture of Sec. III A) are released very close to the respective maxima of U_{eff}, and this is what Eq. (50) actually describes, see App. A.

This brings us to another test of the liquid drop picture: as $\omega \to \omega_{\min}$ we expect the "edge" of the Q-ball to become more and more well-defined. We have seen this in Fig. 7, but this observation can be made quantitative by defining the thickness of the edge region as

$$(\Delta r_s^2)^2 = \langle\langle (r^2 - \langle\langle r^2 \rangle\rangle)^2 \rangle\rangle = \langle\langle r^4 \rangle\rangle - \langle\langle r^2 \rangle\rangle^2 \geq 0 \quad (51)$$

where we introduced, c.f. App. C

$$\langle\langle r^n \rangle\rangle = \frac{\int_0^\infty \mathrm{d}r\; r^n s(r)}{\int_0^\infty \mathrm{d}r\; s(r)}\,. \qquad (52)$$

With this definition we can formulate the expectation that in the "thin wall limit" the relative size of the "edge region" vanishes

$$\lim_{\omega \to \omega_{\min}} \frac{\Delta r_s^2}{\langle r_s^2 \rangle} \to 0\,. \qquad (53)$$

This is supported by the numerical results, see Fig. 9.

Finally we turn our attention to the behavior of integrated quantities for $\omega \to \omega_{\min}$. In this limit Q, M, d_1 and the radii diverge, as shown in Fig. 5, although certain ratios of these quantities remain finite, and follow the predictions from the liquid drop picture, see the discussion above. The key to understand quantitatively the behavior of these quantities in the limit $\omega \to \omega_{\min}$ is the surface tension γ, the only "integrated" Q-ball property which remains finite in this limit.
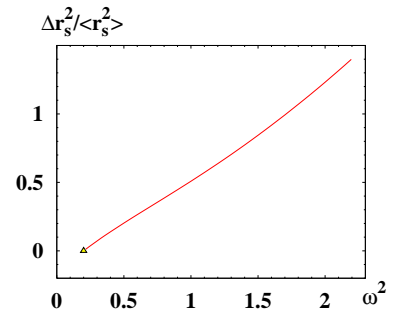

FIG. 9: The ratio $\Delta r_s^2/\langle r_s^2 \rangle$ characterizing the relative size of the "wall thickness," as function of ω^2 (solid line). In the limit $\omega \to \omega_{\min}$ ("thin-wall limit") $\Delta r_s^2/\langle r_s^2 \rangle \to 0$ (marked by the symbol). The numerical results support this expectation.
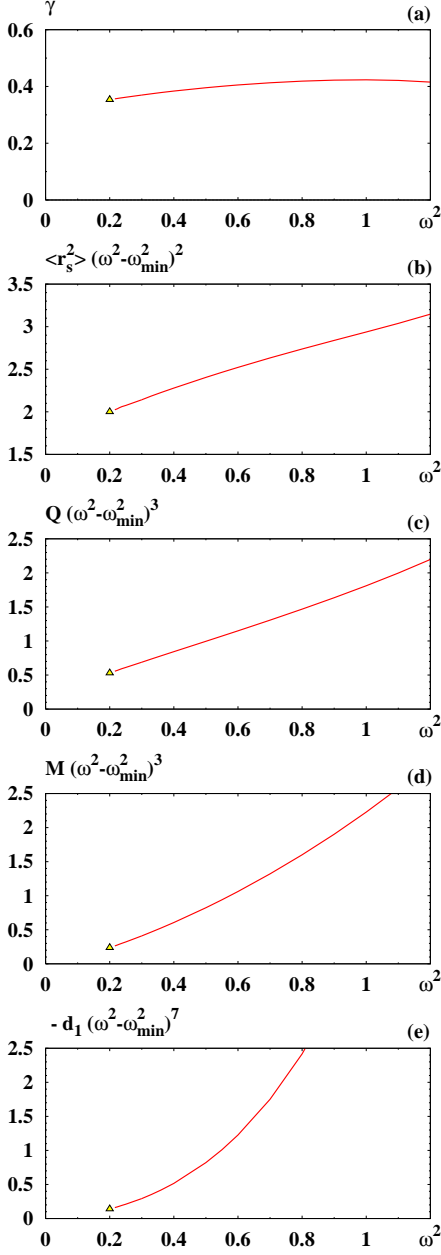
FIG. 10: Q-ball properties as functions of ω^2 plotted in the form $X(\omega^2 - \omega_{\min}^2)^N$. The respective quantities X, and their scaling powers N, written as the pairs (X, N), are as follows: (a) $(\gamma, 0)$, (b) $(\langle r_s^2 \rangle, 2)$, (c) $(Q, 3)$, (d) $(M, 3)$, (e) $(d_1, 7)$. The triangles mark the analytical predictions from Eqs. (57, 59, 60, 61, 62).

The surface energy E_{surf} diverges because it is proportional to the surface area, which diverges for $\omega \to \omega_{\min}$. Taking out carefully these divergences allows one to define the surface tension, cf. Eq. (2.19) in [25], as

$$\lim_{\omega \to \omega_{\min}} \gamma = \lim_{\omega \to \omega_{\min}} \int_0^{\phi_0} d\phi \ \sqrt{2\hat{U}} \,, \quad (54)$$

where $\hat{U} = V(\phi) - \frac{1}{2}\omega^2\phi^2$. Let us define

$$\varepsilon_{\min} = \sqrt{\omega^2 - \omega_{\min}^2} > 0 \,. \quad (55)$$

With the substitution $\phi \to x = \phi^2$ we obtain

$$\int_0^{\phi_0} d\phi \ \sqrt{2\hat{U}} \equiv \frac{1}{2} \int_0^{\phi_0^2(\varepsilon_{\min})} dx \ \sqrt{2C\left(\frac{B}{2C} - x\right)^2 - \varepsilon_{\min}^2} \quad (56)$$

For $\varepsilon_{\min} \neq 0$ the integrand is complex. Recalling that for $\varepsilon_{\min} \to 0$ we have $\phi_0^2(\varepsilon_{\min}) \to \phi_{\mathrm{const}}^2 = B/(2C)$, see App. A, we obtain, for our parameters,

$$\lim_{\omega \to \omega_{\min}} \gamma = \frac{\sqrt{C}}{2\sqrt{2}} \left(\frac{B}{2C}\right)^2 = \frac{1}{2\sqrt{2}} \,, \quad (57)$$

which agrees with the numerical results, see Fig. 10a.

Next we want to determine the behavior of the mean square radius $\langle r_s^2 \rangle$ in this limit. From Eq. (50) we obtain for $p(0)$, Eq. (17), the behavior

$$p(0) = \frac{1}{2}\omega^2\phi_0^2 - V(\phi_0) = \frac{B}{4C}\varepsilon_{\min}^2 + \mathcal{O}(\varepsilon_{\min}^4) \,, \quad (58)$$

which we have seen in Fig. 8d and derived alternatively in App. B. Combining this result with (46, 57) yields for our potential

$$\lim_{\varepsilon_{\min} \to 0} \varepsilon_{\min}^4 \langle r_s^2 \rangle = \frac{B^2}{2C} = 2 \,, \quad (59)$$

which is supported by the numerical results in Fig. 10b. Analogously we obtain

$$\lim_{\varepsilon_{\min} \to 0} \varepsilon_{\min}^6 Q = \frac{\pi}{3\sqrt{2}} \frac{B^4}{C^{5/2}} \omega_{\min} \,, \quad (60)$$

$$\lim_{\varepsilon_{\min} \to 0} \varepsilon_{\min}^6 M = \frac{\pi}{3\sqrt{2}} \frac{B^4}{C^{5/2}} \omega_{\min}^2 \,, \quad (61)$$

$$\lim_{\varepsilon_{\min} \to 0} \varepsilon_{\min}^{14} d_1 = -\frac{\pi^2}{144} \frac{B^{10}}{C^6} \omega_{\min}^2 \,. \quad (62)$$

The numerical results in Figs. 10c–e fully support these conclusions. We see that among the quantities in (57–62) d_1 has the most rapid rise for $\omega \to \omega_{\min}$, which explains the observations in Fig. 5. Combining (59, 61, 62) yields

$$\frac{d_1}{M^2 \langle r_s^2 \rangle} = -\frac{1}{4} \frac{\varepsilon_{\min}^2}{\omega_{\min}^2} + \dots \,, \quad (63)$$

where the dots indicate higher order terms. Eq. (63) explains the observation made in Fig. 6, namely that d_1 measured in its "natural units" vanishes in this limit.

The liquid drop analogy was very successful. One could be tempted to drive it further than we did it here, e.g., by giving the drop also a uniform charge distribution. The resulting repulsive forces ensure stability, and a virial theorem analog to (29) can be derived. But the microscopic details of the stabilizing dynamics are different from a Q-ball, and we will not pursue this analogy further.

V.   THE LIMIT $\omega \to \omega_{\max}$

In this section we discuss the properties of Q-balls for $\omega \to \omega_{\max}$. For certain potentials one obtains small and stable Q-balls in this so-called "thick-wall" limit [30]. But in our potential for $\omega^2 > \omega_c^2 \approx 1.9$ the Q-balls are unstable. For instance, the solution $\omega^2 \approx 2.192$ with $Q = 42$ and $M \approx 62.4$ can decay into 2 absolutely stable Q-balls corresponding to $\omega^2 \approx 1.223$ with $Q = 21$ and $M \approx 28.5$, or into 3 absolutely stable Q-balls corresponding to $\omega^2 \approx 1.466$ with $Q = 14$ and $M \approx 20.4$.[1]

Finally, as $\omega \to \omega_{\max}$ in our potential, the solutions get more and more spread out, and approach from above $M \to mQ$ where $m = \omega_{\max}$ is the mass of the quanta, see Fig. 4. This means that the unstable Q-balls dissociate into a gas of free quanta, a "Q-cloud" [28].

The aim of this section is to study analytically how Q-ball properties behave for $\omega \to \omega_{\max}$. The key for that is the large-r asymptotics of $\phi(r)$ derived in Eq. (10) which shows that as long as $\omega^2 < \omega_{\max}^2$ the solutions $\phi(r)$ decay at large r fast enough to ensure the convergence of the integrals appearing in M, Q, or other properties. Of course, the existence condition (7) requires ω to be always smaller than $\omega_{\max}$. But we may study the scaling of Q-ball properties as ω approaches $\omega_{\max}$ from below.

Let us define

$$\phi_{\mathrm{asymp}}(r) = \frac{c_\infty}{r}\, e^{-\varepsilon_{\max} r}\,, \quad \varepsilon_{\max} = \sqrt{\omega_{\max}^2 - \omega^2} > 0,$$
(64)

which is the leading term in the large-r asymptotics of $\phi(r)$ in (10). We consider first the charge Q in Eq. (6)

$$\begin{aligned}
Q &= 4\pi\,\omega \int_0^\infty \mathrm{d}r\, r^2 \phi^2(r) \\
&\approx \ldots + 4\pi\,\omega \int_{\ldots}^\infty \mathrm{d}r\, r^2 \phi_{\mathrm{asymp}}^2(r) \\
&= \ldots + \frac{4\pi\,\omega\, c_\infty^2}{\varepsilon_{\max}} \int_{\ldots}^\infty \mathrm{d}x\, \exp(-2x)\,,
\end{aligned}$$
(65)

where in the second step we split the integral into an inner (indicated by the three dots) and an outer part. It is understood that this decomposition is done at a sufficiently large radius R such that $\phi(r)$ can be well approximated by its asymptotic form (64) for $r > R$. In the third step in (65) we made the substitution $r \to x = \varepsilon_{\max} r$.

From Eq. (65) we see what happens as $\varepsilon_{\max}$ decreases. The inner part indicated by the three dots in (65) gives a
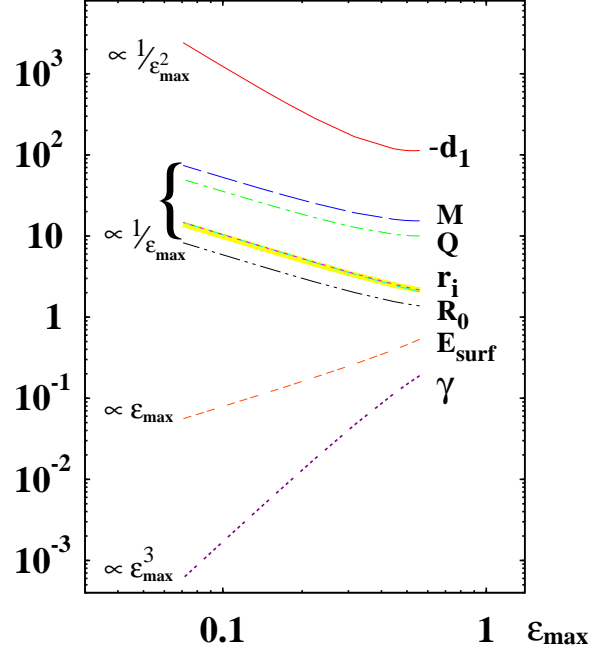

FIG. 11: The Q-ball properties d_1, M, Q, R_0, $r_i = \langle r_i^2 \rangle^{1/2}$ ($i = E$, Q, s), E_{surf}, γ as functions of $\varepsilon_{\max} = \sqrt{\omega_{\max}^2 - \omega^2}$. The region in the plot covers the range $1.8 \le \omega^2 \le 2.195$. The small-$\varepsilon_{\max}$ scaling of d_1, M, Q, $\langle r_Q^2 \rangle^{1/2}$ and $\langle r_E^2 \rangle^{1/2}$ was predicted analytically in Eqs. (66–69).

finite contribution to Q, but the outer contribution scales like $1/\varepsilon_{\max}$. Thus, we expect that with decreasing $\varepsilon_{\max}$ the product $\varepsilon_{\max}Q \to$ const. This method though does not allow us to determine the value of the constant. For that a more careful analysis is needed, which we will report elsewhere [47]. But in this way we correctly predict that $Q \propto 1/\varepsilon_{\max}$ at small $\varepsilon_{\max}$, which is fully supported by the numerical results, see Fig. 11.

Applying this method to other quantities we obtain the results summarized below (all constants are positive and different in each case)

$$\lim_{\varepsilon \to 0} \varepsilon_{\max} Q = \mathrm{const},$$
(66)

$$\lim_{\varepsilon \to 0} \varepsilon_{\max} M = \mathrm{const},$$
(67)

$$\lim_{\varepsilon \to 0} \varepsilon_{\max}^2 d_1 = -\mathrm{const},$$
(68)

$$\lim_{\varepsilon \to 0} \varepsilon_{\max}^2 \langle r_k^2 \rangle = \mathrm{const}, \quad k = Q, E, s,$$
(69)

$$\lim_{\varepsilon \to 0} \varepsilon_{\max}^{-1} E_{\mathrm{surf}} = \mathrm{const}\,,$$
(70)

$$\lim_{\varepsilon \to 0} \varepsilon_{\max}^{-3} \gamma = \mathrm{const}\,.$$
(71)

The predictions (66–71) are fully supported by the numerical results as shown in Fig. 11.

Notice that the results (69–71) for E_{surf}, γ, $\langle r_s^2 \rangle$ are numerical observations, because our method cannot be applied to quantities vanishing with $\varepsilon_{\max} \to 0$. In fact, for instance the scaling of the outer contribution in the integral (27) defining E_{surf} does imply Eq. (70). But our

---

[1] Here we content ourselves to state that the decays are possible energetically, but we are not concerned about their dynamics. Notice also that in these examples integer charges were chosen. But in general the charge Q is not quantized. Also "asymmetric" decays into Q-balls of different charges are possible, but then less energy is released.

rough method would generically suggest that the contribution of the inner region scales like $\varepsilon_{\max}^0$ and dominates. A more careful analysis is needed to prove the prediction (70), see [47]. The same reservations apply to the scaling behavior of γ and $\langle r_s^2 \rangle$, which are both connected to E_{surf} via Eq. (34).

We observe numerically that the position R_0 where $p(r)$ changes sign scales in the same way as the square roots of the mean square radii in (69). Thus, independently of whether we measure it in terms of R_0 or the $\langle r_i^2 \rangle^{1/2}$, the size of the solutions grows with $\varepsilon_{\max} \to 0$.

The constant d_1 diverges as $1/\varepsilon_{\max}^2$ with decreasing $\varepsilon_{\max}$, see Fig. 11. However, when measured in its natural units it actually goes to zero as $d_1/(M^2 \langle r_s^2 \rangle) \propto \varepsilon_{\max}^2$ as we have seen previously in Fig. 6.

To summarize, as $\varepsilon_{\max} \to 0$ mass, charge and size of the Q-balls diverge as $1/\varepsilon_{\max}$, see (66, 67, 69). Thus, the mean charge and energy densities, which are proportional to $Q/(\text{size})^3$ and $M/(\text{size})^3$, vanish like $\varepsilon_{\max}^2$. Fig. 4 has shown that the Q-balls are unstable, and their (positive) binding energy $M - mQ$ approaches zero (from above) as $\varepsilon_{\max} \to 0$. Hence, in this limit we obtain a dilute gas of free Q-quanta as discussed in [28].

VI. THE SIGN OF d_1

In this section we will show in several independent ways that d_1 is negative. In Sec. VI A we will use for that the observation that for Q-balls $s(r)$ *happens* to be positive for $0 < r < \infty$, and in Sec. VI B we will explain why $s(r)$ *must* be positive. In Sec. VI C we will prove that $d_1 < 0$ using arguments based on $p(r)$ and the Laue condition.

One may wonder why several proofs are needed. Indeed, the EMT conservation dictates that $s(r)$ and $p(r)$ are connected by the differential equation (20), which is the origin of the equivalent presentations (18, 19) for d_1 in terms of $s(r)$ and $p(r)$ [16], and we have explicitly proven that our expressions for $s(r)$ and $p(r)$ satisfy (20). So, if one is able to conclude from $s(r)$ the sign of d_1, then it must be possible to draw the same conclusion also from $p(r)$. Therefore, at first glance it may seem sufficient to conclude the sign of d_1 in one way, and below we will see that for Q-balls it is much easier to use $s(r)$ for that.

However, concluding the sign of d_1 from $s(r)$ alone bears some danger, because from *any* "input" $s(r)$ one obtains via (20) a function $p(r)$ which automatically[2] satisfies the Laue condition (22) [16]. So one may well encounter an approach with $s(r) \geq 0$ and conclude $d_1 < 0$ *without* being sure one really deals with a correct solution of the equations of motion and a true minimum

of the energy functional. But the other way round, the pressure is ultimately related to the issue of stability by Eq. (22), which we have shown to be equivalent to the virial theorem (29). A proof that $d_1 < 0$ on the basis of $p(r)$ is therefore in general on a much more solid ground.

A. Arguments based on $s(r)$ and inequalities

In this section we will show that $d_1 < 0$ using arguments based on the shear force distribution. The argument is trivial and makes use of the observation that manifestly $s(r) = \phi'(r)^2 \geq 0 \ \forall r$.

In Eq. (18) we have seen that d_1 is given by $(-\frac{4}{3}\pi M)$ times the integral over $r^4 s(r)$ over r from zero to infinity. Since $s(r) \geq 0$ this immediately implies $d_1 \leq 0$. This inequality can be improved by recalling that $\phi'(r) < 0$ for $0 < r < \infty$, see Sec. III A. Therefore $d_1 < 0$ which completes the proof.

The fact that $s(r) \geq 0$ can be further explored to derive an inequality showing that d_1 must be negative. Using (51, 52) we have $d_1 = -\frac{4\pi}{3} M \gamma \langle\langle r^4 \rangle\rangle$ and $\langle r_s^2 \rangle = \langle\langle r^2 \rangle\rangle$ and can rewrite the constant d_1 as

$$ -\frac{d_1}{M^2 \langle r_s^2 \rangle} = \frac{M - \omega Q}{M} \left(1 + \left(\frac{\Delta r_s^2}{\langle r_s^2 \rangle} \right)^2 \right). \tag{72} $$

Notice we implicitly benefited from the fact that $s(r) \geq 0$, when introducing the averages $\langle\langle r^n \rangle\rangle$ in (52). Next we explore that $E_{\text{surf}} = \int d^3 r \, s(r) > 0$, and with $\omega Q > 0$ we conclude from (30) that $0 < M - \omega Q < M$. Using the latter inequality in (72) finally implies that

$$ 0 < -\frac{d_1}{M^2 \langle r_s^2 \rangle} < 1 + \left(\frac{\Delta r_s^2}{\langle r_s^2 \rangle} \right)^2. \tag{73} $$

This proves that $(-d_1) > 0$. As a byproduct Eq. (73) provides also an upper bound on $(-d_1)$ but in terms of $\Delta r_s^2 / \langle r_s^2 \rangle$. At this point it is not obvious whether this quantity is bound from above, though numerically we observe this to be the case in Fig 9. That $\Delta r_s^2 / \langle r_s^2 \rangle$ is indeed bound from above will be shown in [47].

For completeness let us mention the following more useful upper bound on the magnitude of $(-d_1)$. The starting point is Eq. (35) where we neglect the positive quantity $\omega Q M \langle r_Q^2 \rangle = M \omega^2 \int d^3 r \, r^2 \phi(r)^2$. This yields the bound

$$ -\frac{d_1}{M^2 \langle r_E^2 \rangle} < \frac{5}{9}, \tag{74} $$

which is satisfied by the numerical results, see Fig. 6. We checked that this is the strongest inequality one can derive involving $\langle r_E^2 \rangle$ as length scale. The inequality (74) is attractive because it provides an upper bound on $(-d_1)$ in "its natural units" solely in terms of quantities related to the energy density $T_{00}(r)$.

---

[2] The differential equation (20) allows one to determine $p(r)$ from a given input function $s(r)$ only up to an integration constant. But the latter can be fixed by demanding that for a well-localized finite-energy object $p(r) \to 0$ as $r \to \infty$. In a similar way one can determine $s(r)$ from a given input function $p(r)$.

B. Arguments based on the particle interpretation

In the previous section we explored the observation that $s(r)$ *happens* to be positive for $0 < r < \infty$ for Q-balls. Here we will show this *must* be the case.

For that we use the particle interpretation picture [25] discussed in Sec. III A. The Newtonian equation (39) describing the motion of a unit mass particle moving in the effective potential $U_{\rm eff} = \frac{1}{2}\omega^2 x^2 - V(x)$ under the friction $F_{\rm fric} = -\frac{2}{t}\dot{x}(t)$ follows from the Langrange-function $L(\dot{x}, x)$ and Rayleigh's dissipation function $\mathcal{F}(\dot{x})$,

$$ L(\dot{x}, x) = \frac{1}{2}\,\dot{x}(t)^2 - U_{\rm eff}(x), \quad \mathcal{F}(\dot{x}) = \frac{1}{t}\,\dot{x}(t)^2, \quad (75) $$

according to

$$ \frac{\rm d}{{\rm d}t}\left(\frac{\partial L}{\partial \dot{x}}\right) - \frac{\partial L}{\partial x} = -\frac{\partial \mathcal{F}}{\partial \dot{x}}. \quad (76) $$

The physical meaning of Rayleigh's dissipation function $\mathcal{F}(\dot{x})$ is that it describes the rate at which the system dissipates its energy E due to the frictional force, namely

$$ \frac{{\rm d}E}{{\rm d}t} = \frac{\rm d}{{\rm d}t}\left(\partial \dot{x}\,\frac{\partial L}{\partial \dot{x}} - L\right) = -2\,\mathcal{F} \leq 0 \quad \forall\, t, \quad (77) $$

which must be negative because the system *dissipates* energy. This means that $\mathcal{F}(\dot{x}) \geq 0 \ \forall\, t$.

If we recall that $x(t)$ and t in the particle interpretation picture correspond to $\phi(r)$ and r, we instantly see that $\mathcal{F}(\dot{x})$ corresponds to $\frac{1}{r}\,s(r)$. Since $\mathcal{F}(\dot{x}) \geq 0$ this proves that the distribution of shear forces $s(r) \geq 0$.

C. Arguments based on the pressure $p(r)$

In this section we will prove that d_1 is negative, basing our arguments on the pressure distribution.

Let us first demonstrate that for ω satisfying the existence condition (7) the pressure is positive at small r, and negative at large r. In Sec. III A we have proven $p(0) > 0$, and for reasons of continuity $p(r) > 0$ also in some vicinity of the origin. At large-r we derive from (10) the following asymptotics for the pressure

$$ p(r) = -(\omega_{\rm max}^2 - \omega^2)\,\frac{2\,c_\infty^2}{3\,r^2}\,\exp\left(-2\,r\,\sqrt{\omega_{\rm max}^2 - \omega^2}\right) + \dots \quad (78) $$

where the dots indicate subleading terms. Clearly, for all ω satisfying the existence condition (7), the pressure is negative at large r. To summarize, we have

$$ \begin{aligned} p(r) &> 0 \quad \text{for small } r, \\ p(r) &< 0 \quad \text{for large } r. \end{aligned} \quad (79) $$

This implies that $p(r)$ must change the sign an odd number of times. Of course, $p(r)$ must change sign at least to comply with the Laue condition (22). From physical

point of view, we expect $p(r)$ to be positive in the center (which implies repulsive forces directed towards outside) and negative outside (attractive forces towards inside), as we derived in (79). A stable solution arises when the repulsive and attractive forces exactly balance each other according to (22). This physically intuitive pattern was observed also in soliton models of the nucleon [16–19].

For a ground state one may expect the pressure distribution to change sign only once, see Fig. 2d. If we *assume* $p(r)$ to change sign one and only one time, this immediately implies that d_1 is negative. Fig. 12 illustrates the argument. The left panel of Fig. 12 visualizes the Laue condition (22): the shaded areas above and below the x-axis are equal and exactly compensate each other. Thus, due to the Laue condition (22) we have

$$ \int_0^{R_0} {\rm d}r \underbrace{R_0^2\,r^2}_{>\,r^4}\,p(r) = -\int_{R_0}^\infty {\rm d}r \underbrace{R_0^2\,r^2}_{<\,r^4}\,p(r) $$

$$ \Rightarrow \quad \int_0^{R_0} {\rm d}r\,r^4 p(r) < -\int_{R_0}^\infty {\rm d}r\,r^4 p(r) \quad (80) $$

which means $\int_0^\infty {\rm d}r\,r^4 p(r) < 0$, and d_1 must be negative, as can be seen in the right panel of Fig. 12.

If we knew $p(r)$ has one zero only, the proof that $d_1 < 0$ would be complete here. It is intuitive to assume that the pressure distribution of a ground state changes sign only once according to (79). However, here we will provide a general argument which is valid not only for ground states.

For that we need the following lemma. For any solution of the Q-ball equations of motion we have

$$ \int_0^R {\rm d}r\,r^2\,p(r) > 0 \quad \text{for} \quad 0 < R < \infty. \quad (81) $$

To prove (81) we make use of the result (25) derived in Sec. II C and explore the particle interpretation picture of the Q-ball equations of motion. For that we notice that $p(r) + \frac{2}{3}\,s(r)$, the right-hand-side of (25), is positive $\forall\, r < \infty$ because

$$ \left(p(r) + \frac{2}{3}\,s(r)\right) = \underbrace{\frac{1}{2}\,\phi'(r)^2}_{E_{\rm kin}} + \underbrace{\frac{1}{2}\omega^2\phi(r)^2 - V(\phi)}_{U_{\rm eff}}. \quad (82) $$

In other words, $p(r) + \frac{2}{3}\,s(r)$ corresponds to the total, kinetic plus potential, energy of the particle at a given time t (with $t \leftrightarrow r$). The total energy of the particle must be larger than zero $\forall\, t < \infty$, because at any finite time t the particle still needs to do work against the friction in order to arrive, after infinite time, at the origin $x = 0$ (with $x \leftrightarrow \phi$). This means that the integral in (25) is positive and proves Eq. (81).

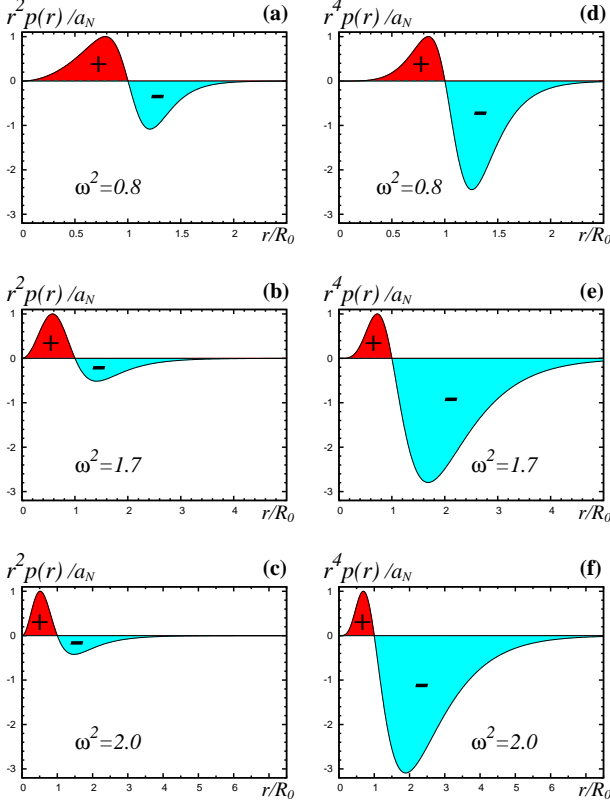To understand this result intuitively, we remark that if the integral (81) could become zero at some finite R,

FIG. 12: $r^2 p(r)$ and $r^4 p(r)$ as functions of r for selected ω. For better comparison, r is given in units of the radius R_0 where $p(r)$ changes sign, and the normalization factors a_N are such that the curves reach unity at their global maxima. The left (right) panel shows the integrand of the Laue condition (the integrand of d_1, Eq. (19), up the prefactor $5\pi M$). The figure illustrates why d_1 is negative. Integrating the curves in the left panel yields zero due to (19). Weighting the curves by an additional factor of r^2 and integrating then yields a negative result for d_1, see right panel.

then the fields would stabilize themselves in a subinterval $r \in [0, R]$. Then, setting the fields outside that interval to zero, would yield a stable solution with lower mass (because $T_{00}(r) \geq 0$ also in the omitted region), in contradiction to the expectation that a given set of initial value data leads to a unique minimum of the action.

We have now all ingredients for the proof that $d_1 < 0$ based on pressure and the Laue condition, namely (79) and (81). The proof is as follows.

Eq. (79) means $p(r)$ must change sign an odd number N of times. Let R_i with $i = 1, \ldots, N$ denote the radii where this happens with $0 < R_1 < R_2 < \ldots < R_N < \infty$. Notice that we do not include points where $p(r)$ could have zeros without changing sign.

The Laue condition (22) can then be written as

$$\int_0^{R_1} dr\, r^2 p(r) + \int_{R_1}^{R_2} dr\, r^2 p(r) + \ldots + \int_{R_N}^{\infty} dr\, r^2 p(r) = 0 \,. \quad (83)$$

By construction $p(r) \geq 0$ in the first, third, ... integrals,

and $p(r) \leq 0$ in the second, fourth, ... last integrals. We will now replace each of the terms in (83) by a smaller term, and show in this way that $\int_0^{\infty} dr\, r^4 p(r) < 0$.

Step 1. We consider the first 2 terms in (83). In the first (second) term $p(r)$ is positive (negative). Therefore

$$\int_0^{R_1} dr\, r^2 p(r) \geq \frac{1}{R_1^2} \int_0^{R_1} dr\, r^4 p(r)\,,$$

$$\int_{R_1}^{R_2} dr\, r^2 p(r) \geq \frac{1}{R_1^2} \int_{R_1}^{R_2} dr\, r^4 p(r)\,. \quad (84)$$

Adding up the 2 inequalities in (84) we obtain

$$\int_0^{R_2} dr\, r^2 p(r) \geq \frac{1}{R_1^2} \int_0^{R_2} dr\, r^4 p(r) \,. \quad (85)$$

If there is only one change of sign, then we take the limit $R_2 \to \infty$ and recover the situation of Eq. (80), and our proof is complete here. If $p(r)$ changes sign more than once, i.e. $N \geq 3$, then we have to continue our proof and include further contributions in step 2.

Step 2. Notice that $\int_0^{R_2} dr\, r^4 p(r) > 0$ for $R_2 < \infty$ due to (81). Moreover $R_1 < R_3 < \infty$. Therefore

$$\int_0^{R_2} dr\, r^2 p(r) \geq \frac{1}{R_1^2} \int_0^{R_2} dr\, r^4 p(r) > \frac{1}{R_3^2} \int_0^{R_2} dr\, r^4 p(r) \,. \quad (86)$$

In the next two intervals $p(r) \geq 0$ for $r \in [R_2, R_3]$, and $p(r) \leq 0$ for $r \in [R_3, R_4]$. Therefore, in analogy to (84),

$$\int_{R_2}^{R_3} dr\, r^2 p(r) \geq \frac{1}{R_3^2} \int_{R_2}^{R_3} dr\, r^4 p(r)\,,$$

$$\int_{R_3}^{R_4} dr\, r^2 p(r) \geq \frac{1}{R_3^2} \int_{R_3}^{R_4} dr\, r^4 p(r)\,. \quad (87)$$

Combining (86) and the results in (87) we obtain

$$\int_0^{R_4} dr\, r^2 p(r) > \frac{1}{R_3^2} \int_0^{R_4} dr\, r^4 p(r) \,. \quad (88)$$

If $p(r)$ changes sign exactly $N = 3$ times, then we take in (88) the limit $R_4 \to \infty$ and our proof is completed here. If $p(r)$ changes sign more often, then we repeat step 2.

Last step. If $p(r)$ changes the sign $N = 2k + 1$ times (recall that N is odd, and $R_N < \infty$), then we repeat successively the 2nd step k-times, until we arrive at

$$\int_0^{\infty} dr\, r^2 p(r) > \frac{1}{R_N^2} \int_0^{\infty} dr\, r^4 p(r) \,. \quad (89)$$

Now, the first integral vanishes due to the Laue condition (22), and using the definition (19) giving d_1 in terms of the pressure, we conclude from (89) the desired result that d_1 must be negative.

D. Stability and d_1

Above we have proven $d_1 < 0$ exploring the Laue condition which is satisfied by all solutions, minimizing the energy functional, see Sec. II C. It is important to stress that thereby we did not use the stability considerations discussed in Sec. II A. All solutions correspond to minima of the energy functional and therefore must have $d_1 < 0$. Whether the minima are global or local, and whether they describe stable, meta-stable or unstable Q-balls plays no role for the sign of d_1. Fig. 12 illustrates this point: the solutions in Figs. 12a, b, c are respectively stable, metastable and unstable. But in all cases d_1 is negative, as shown in Figs. 12d–e.

VII. CONCLUSIONS

We have presented a study of Q-balls in a scalar field theory with U(1) symmetry, and investigated the properties of Q-balls as functions of the angular velocity ω. While Q-ball stability was studied in literature before [37–42], to best of our knowledge this is the first study in which this issue is addressed from the point of view of the EMT, and the constant d_1. All solutions presented in this work were exact solutions of the equations of motion. Particular focus was put on the behavior of Q-ball properties for ω approaching the boundaries $\omega_{\min,\max}$ of the region in which solutions exist.

For $\omega \to \omega_{\min}$ the Q-balls occupy increasingly large volumes filled with Q-ball matter of nearly constant density [25]. We have shown that in this limit the Q-ball properties follow the predictions of the liquid drop picture. Certain Q-ball properties such as charge Q, mass M, mean square radii, and d_1 diverge as $\omega \to \omega_{\min}$. We derived analytically the limits for these and other properties, which are fully supported by our numerical results.

In the opposite limit $\omega \to \omega_{\max}$ the solutions become unstable and approach the "Q-cloud limit" [28]. Also in this limit some properties diverge. We derived analytically the scaling behavior of these quantities as ω approaches $\omega_{\max}$. Further results will be reported in [47]. It is remarkable that, among all properties we studied, d_1 diverges most strongly as $\omega \to \omega_{\min,\max}$.

The conservation of the EMT implies among others the Laue condition [4, 48] which states that the pressure must satisfy $\int_0^\infty \mathrm{d}r\, r^2 p(r) = 0$, which we have proven explicitly in two independent ways. One of the proofs is equivalent to the virial theorem.

The central result of this work is that the constant d_1 is strictly negative for all Q-ball solutions,

$$d_1 < 0 \,, \tag{90}$$

for which we have provided 2 explicit analytical proofs. One proof involved the relation of d_1 to $s(r)$, and made use of the Newtonian particle interpretation of the Q-ball equations of motion [25] in which the shear force distribution $s(r)$ is related to the Rayleigh dissipation function describing the frictional forces. Since the Newtonian system dissipates energy due to friction, $s(r)$ must be positive for $0 < r < \infty$. This implies $d_1 < 0$.

The other proof explored the relation of d_1 to $p(r)$, and made use of the Laue condition. We have shown, using the equations of motion, that $p(r)$ is positive in the center of the Q-ball (which corresponds to repulsion) and negative at large r (which corresponds to attraction). This means $p(r)$ must change the sign an odd number of times, and we have formulated a general proof valid for any Q-ball solution with a pressure with an arbitrary number of zeros. We observed that for ground states $p(r)$ changes sign only once, but for radial excitations of Q-balls one encounters more complex structures [47].

The proof of (90) based on $p(r)$ elucidates that for Q-balls the negative sign of d_1 is a consequence of the Laue condition. The last important insight of our study is that $d_1 < 0$ holds not only for stable solutions. In the Q-ball system $d_1 < 0$ holds also for meta-stable and unstable solutions, for which no study of d_1 has been previously presented in literature. This indicates that $d_1 < 0$ could hold for all particles, irrespective of whether they are stable or unstable. Since d_1 is not known experimentally for any particle, this is already an important information.

Interesting open questions are whether d_1 of rotating Q-balls [37, 38] is also negative, and how quantum fluctuations [51] modify the picture of d_1. It would be also interesting to see how d_1 is altered for Q-balls coupled to fermionic fields, which allows them to 'evaporate' [27]. The ultimate goal would be to generalize the proofs given in this work to quantum field theories, and to apply them to the description of hadrons. So far, in all theoretical studies d_1 was always found negative, for pions [13], nucleons [15–19], and nuclei [4, 20, 21]. Also lattice QCD calculations yield a negative quark contribution to the d_1 of nucleon, though the gluon contribution and hence the total d_1 are not yet known [14]. First experimental results are compatible with d_1 being negative [52] but this observation is not yet conclusive [53], and future data will provide further insights [54].

Appendix A: Stationary solutions

In this Appendix we discuss stationary solutions of the equations of motion (4, 5) of the type $\phi(r) = \phi_{\mathrm{const}}\ \forall r$. Though they do not obey the boundary condition (5) at infinity, these solutions are nevertheless of interest.

If $\phi(r) = \phi_{\mathrm{const}}$ the boundary conditions at $r = 0$ in (5) hold, and the equation of motion (4) becomes

$$\omega^2 \phi_{\mathrm{const}} - V'(\phi_{\mathrm{const}}) \tag{A1}$$

$$= \left(\omega^2 - 2A + 4B\phi_{\text{const}}^2 - 6C\phi_{\text{const}}^4 \right) \phi_{\text{const}} = 0.$$

The trivial solution $\phi_{\text{const}} = 0$ describes the vacuum. Further (for $\omega_{\min} \leq \omega \leq \omega_{\max}$ always real) solutions are

$$\phi_{\text{const}}^2 = \frac{B}{3C} \pm \left(\frac{B^2}{9C^2} + \frac{\omega^2 - 2A}{6C} \right)^{1/2} . \qquad \text{(A2)}$$

Because $\mathcal{L}$ in (1) is symmetric under $\phi \to -\phi$ it is sufficient to focus on the non-negative solutions.

In the particle interpretation picture the two positive stationary solutions in (A2) have the following meaning. The solution with the minus-sign in (A2) corresponds to the situation that the particle is at $t = 0$ precisely in the local minimum of the effective potential in Fig. 1 and will stay there forever. The solution with the plus-sign in (A2) corresponds to the (not stable) situation that the particle is at $t = 0$ precisely in the global maximum of the effective potential in Fig. 1 and will stay there forever.

As $\omega \to \omega_{\min}$ we obtain $\phi_{\text{const}}^2 = B/(6C)$ from (A2), which corresponds to the (not interesting for us) situation where the particle stays forever in the minimum of U_{eff}, and the (much more interesting) solution

$$\phi_{\text{const}}^2 \to \frac{B}{2C} = 1 \quad \text{as} \quad \omega \to \omega_{\min}, \qquad \text{(A3)}$$

which corresponds to the situation with the particle placed at the maximum of $U_{\text{eff}}(\phi)$ which for ω approaching $\omega_{\min}$ from above is just above zero. This situation is of interest, because as $\omega \to \omega_{\min}$ the particle has to be placed very close to this maximum of $U_{\text{eff}}(\phi)$, and "wait" there long enough such that its small initial potential energy $U_{\text{eff}}(\phi)$ is sufficient to overcome the time-dependent friction which decreases with time [25].

As $\omega \to \omega_{\max}$ we obtain from (A2) the solutions $\phi_{\text{const}}^2 = 0$ and $\phi_{\text{const}}^2 = (2B)/(3C)$. When $\omega = \omega_{\max}$ the effective potential does not dip below zero at all, i.e. it is not possible to release the particle from any $\phi_0 > 0$ so it would stop in the origin [25]. The only solution is $\phi_{\text{const}}^2 = 0$. However, from (A2) that solution develops in the limit $\omega \to \omega_{\max}$ from the minimum of U_{eff} which is below zero. But for any regular solution with $\omega < \omega_{\max}$ the potential at the starting point $U_{\text{eff}}(\phi_0) > 0$. Therefore, the stationary solution $\phi_{\text{const}}^2 = 0$ obtained here is not continuously connected to the limiting value for ϕ_0 stated in Eq. (41).

Appendix B: Bounds on the pressure

The pressure at the origin is just $p(0) = U_{\text{eff}}(\phi_0)$ and this is positive, Eq. (40), because for any regular solution the effective potential of the particle at the starting point must be positive. In this Appendix we will show that the pressure is also bound from above. From (5, 17) we obtain

$$p(0) = \frac{1}{2} \omega^2 \phi_0^2 \left(1 - \frac{2V(\phi_0)}{\omega^2 \phi_0^2} \right) . \qquad \text{(B1)}$$

Using (8) we notice that $\forall \phi(r)$ (including $\phi(r)$ at $r = 0$)

$$\frac{2V(\phi)}{\phi^2} \geq \min_\phi \left[\frac{2V(\phi)}{\phi^2} \right] \equiv \omega_{\min}^2 . \qquad \text{(B2)}$$

Inserting (B2) in (B1) and including also the lower bound from Eq. (40) we obtain

$$0 < p(0) \leq \frac{1}{2} (\omega^2 - \omega_{\min}^2) \phi_0^2 . \qquad \text{(B3)}$$

An important application of the upper bound in (B3) is that it allows to verify independently the result for $p(0)$ in the limit $\omega \to \omega_{\min}$ quoted in (49). We remark that the upper bound in (B3) is for $\omega_{\min} < \omega < \omega_{\max}$ always a real inequality and saturated only in the limit $\omega \to \omega_{\min}$.

Appendix C: Generating functional for $\langle\langle r^n \rangle\rangle$

In Sec. IV we defined the $\langle\langle r^n \rangle\rangle$ in (52), which allowed us to express compactly $\langle r_s^2 \rangle = \langle\langle r^2 \rangle\rangle$ and the measure for the wall width $(\Delta r_s^2)^2 = \langle\langle r^4 \rangle\rangle - \langle\langle r^2 \rangle\rangle^2$. Another interesting application, if we continue to negative n, is $p(0) = 2\gamma \langle\langle r^{-1} \rangle\rangle$. This allows us to express the result obtained in (46) as

$$\lim_{\omega \to \omega_{\min}} \langle\langle r^{-1} \rangle\rangle \langle\langle r^2 \rangle\rangle^{1/2} = 1. \qquad \text{(C1)}$$

The result in Eq. (C1) can be understood and interpreted by recalling that $s(r) \to \gamma \delta(r - R)$ in the liquid drop limit which is equivalent to $\omega \to \omega_{\min}$, see Sec. IV.

The positivity of the shear forces, which was crucial in Secs. VI A and VI B, allows us to introduce the functional

$$F(\lambda) = \int_0^\infty dr \, s(r) \exp(-\lambda r^2) \qquad \text{(C2)}$$

which is a generating functional for $\langle\langle r^n \rangle\rangle$ for even n

$$F(\lambda) = F(0) \sum_{n=0}^\infty \frac{(-1)^n}{n!} \langle\langle r^{2n} \rangle\rangle \lambda^n \qquad \text{(C3)}$$

The surface tension is just $\gamma = F(0)$, the surface energy is $E_{\text{surf}} = -4\pi F'(0)$ and $d_1 = -\frac{4\pi}{3} M F''(0)$. The mean square radius of the shear forces, and the measure of the wall width Δr_s^2 can be expressed as

$$\langle r_s^2 \rangle = - \left[\frac{\partial}{\partial \lambda} \log F(\lambda) \right]_{\lambda=0} , \qquad \text{(C4)}$$

$$(\Delta r_s^2)^2 = \left[\frac{\partial^2}{\partial \lambda^2} \log F(\lambda) \right]_{\lambda=0} . \qquad \text{(C5)}$$

We remark that each integral over $s(r)$ can be traded for an integral over $p(r)$ by exploring the differential equation (20). For instance, $\gamma = \frac{3}{4} \int_0^\infty dr \, p(r)$ and

$$\langle r_s^2 \rangle = - 6 \frac{\int_0^\infty dr \, r^2 p(r) \log r}{\int_0^\infty dr \, p(r)} . \qquad \text{(C6)}$$

These and further relations were derived in [16] and can be used as cross checks for the numerics.

[1] H. R. Pagels, Phys. Rev. **144** (1965) 1250.
[2] X. D. Ji, Phys. Rev. Lett. **74**, 1071 (1995).
[3] X. D. Ji, Phys. Rev. Lett. **78**, 610 (1997).
[4] M. V. Polyakov, Phys. Lett. B **555** (2003) 57.
[5] R. G. Sachs, Phys. Rev. **126**, 2256 (1962).
[6] X. D. Ji, Phys. Lett. B **254** (1991) 456.
G. A. Miller, Phys. Rev. C **80**, 045210 (2009)
[7] D. Müller *et al.*, Fortsch. Phys. **42**, 101 (1994).
A. V. Radyushkin, Phys. Lett. B **380**, 417 (1996); Phys. Lett. B **385**, 333 (1996); Phys. Rev. D **56**, 5524 (1997).
X. D. Ji, Phys. Rev. D **55**, 7114 (1997). J. C. Collins, L. Frankfurt and M. Strikman, Phys. Rev. D **56**, 2982 (1997).
[8] X. D. Ji, J. Phys. G **24**, 1181 (1998). A. V. Radyushkin, arXiv:hep-ph/0101225. K. Goeke, M. V. Polyakov and M. Vanderhaeghen, Prog. Part. Nucl. Phys. **47**, 401 (2001). M. Diehl, Phys. Rept. **388** (2003) 41. A. V. Belitsky and A. V. Radyushkin, Phys. Rept. **418**, 1 (2005).
[9] C. Adloff *et al.* [H1 Collaboration], Phys. Lett. B **517**, 47 (2001). A. Aktas *et al.*, Eur. Phys. J. C **44**, 1 (2005) F. D. Aaron *et al.*, Phys. Lett. B **659**, 796 (2008); Phys. Lett. B **681**, 391 (2009). S. Chekanov *et al.* [ZEUS Collaboration], Phys. Lett. B **573** (2003) 46; JHEP **0905**, 108 (2009).
[10] A. Airapetian *et al.* [HERMES Collaboration], Phys. Rev. Lett. **87**, 182001 (2001); Phys. Rev. D **75**, 011103 (2007); JHEP **0806**, 066 (2008); JHEP **0911**, 083 (2009); Nucl. Phys. B **829**, 1 (2010); Nucl. Phys. B **842**, 265 (2011).
[11] S. Stepanyan *et al.* [CLAS Collaboration], Phys. Rev. Lett. **87**, 182002 (2001). S. Chen *et al.*, Phys. Rev. Lett. **97**, 072002 (2006). F. X. Girod *et al.*, Phys. Rev. Lett. **100**, 162002 (2008). G. Gavalian *et al.*, Phys. Rev. C **80**, 035206 (2009).
[12] C. Munoz Camacho *et al.* [Jefferson Lab Hall A Collaboration], Phys. Rev. Lett. **97**, 262002 (2006). M. Mazouz *et al.*, Phys. Rev. Lett. **99**, 242501 (2007).
[13] M. V. Polyakov and C. Weiss, Phys. Rev. D **60**, 114017 (1999).
[14] N. Mathur, S. J. Dong, K. F. Liu, L. Mankiewicz and N. C. Mukhopadhyay, Phys. Rev. D **62**, 114504 (2000) P. Hägler *et al.* [LHPC collaboration], Phys. Rev. D **68**, 034505 (2003); Phys. Rev. D **77**, 094502 (2008). J. D. Bratt *et al.*, Phys. Rev. D **82**, 094502 (2010). M. Göckeler *et al.* [QCDSF Collaboration], Phys. Rev. Lett. **92**, 042002 (2004)
[15] V. Y. Petrov *et al.*, Phys. Rev. D **57**, 4325 (1998). P. Schweitzer *et al.*, Phys. Rev. D **66**, 114004 (2002). J. Ossmann *et al.*, Phys. Rev. D **71**, 034011 (2005). M. Wakamatsu, Phys. Lett. B **648**, 181 (2007)
[16] K. Goeke *et al.*, Phys. Rev. D **75**, 094021 (2007)
[17] K. Goeke *et al.*, Phys. Rev. C **75**, 055207 (2007)
[18] C. Cebulla *et al.*, Nucl. Phys. A **794**, 87 (2007)
[19] H.-Ch. Kim, P. Schweitzer, and U. Yakhshiev, arXiv: 1205.5228 [hep-ph].
[20] S. Liuti and S. K. Taneja, Phys. Rev. C **72**, 032201 (2005).
[21] V. Guzey and M. Siddikov, J. Phys. G **32** (2006) 251
[22] J. F. Donoghue and H. Leutwyler, Z. Phys. C **52**, 343 (1991). B. Kubis and U. G. Meissner, Nucl. Phys. A **671**, 332 (2000) [Erratum-ibid. A **692**, 647 (2001)]

J. W. Chen and X. D. Ji, Phys. Rev. Lett. **88**, 052003 (2002) A. V. Belitsky and X. D. Ji, Phys. Lett. B **538**, 289 (2002) S.-I. Ando, J.-W. Chen and C.-W. Kao, Phys. Rev. D **74**, 094013 (2006). M. Diehl, A. Manashov and A. Schäfer, arXiv:hep-ph/0608113.
[23] E. Megias, E. Ruiz Arriola, L. L. Salcedo and W. Broniowski, Phys. Rev. D **70**, 034031 (2004) E. Megias, E. Ruiz Arriola and L. L. Salcedo, Phys. Rev. D **72**, 014001 (2005) W. Broniowski and E. R. Arriola, Phys. Rev. D **78**, 094011 (2008)
[24] R. Friedberg, T. D. Lee and A. Sirlin, Phys. Rev. D **13**, 2739 (1976).
[25] S. R. Coleman, Nucl. Phys. B **262**, 263 (1985) [Erratum-ibid. B **269**, 744 (1986)].
[26] A. M. Safian, S. R. Coleman and M. Axenides, Nucl. Phys. B **297**, 498 (1988).
[27] A. G. Cohen, S. R. Coleman, H. Georgi and A. Manohar, Nucl. Phys. B **272**, 301 (1986).
[28] M. G. Alford, Nucl. Phys. B **298**, 323 (1988).
[29] T. D. Lee and Y. Pang, Phys. Rept. **221**, 251 (1992).
[30] A. Kusenko, Phys. Lett. B **404**, 285 (1997); Phys. Lett. B **405**, 108 (1997). A. Kusenko and M. E. Shaposhnikov, Phys. Lett. B **418**, 46 (1998).
[31] S. Kasuya and M. Kawasaki, Phys. Rev. D **61**, 041301 (2000).
[32] T. Multamaki and I. Vilja, Nucl. Phys. B **574**, 130 (2000). F. Paccetti Correia and M. G. Schmidt, Eur. Phys. J. C **21**, 181 (2001). T. A. Ioannidou, A. Kouiroukidis and N. D. Vlachos, J. Math. Phys. **46**, 042306 (2005).
[33] S. S. Clark, Nucl. Phys. B **756**, 38 (2006). M. Fairbairn, A. C. Kraan, D. A. Milstead, T. Sjostrand, P. Skands and T. Sloan, Phys. Rept. **438**, 1 (2007).
[34] D. P. Clougherty, Phys. Rev. Lett. **96**, 045703 (2006).
[35] M. Schmid and M. Shaposhnikov, Nucl. Phys. B **775**, 365 (2007).
[36] Y. Verbin, Phys. Rev. D **76**, 085018 (2007). B. Hartmann and J. Riedel, arXiv:1204.6239 [hep-th].
[37] M. S. Volkov and E. Wohnert, Phys. Rev. D **66**, 085003 (2002).
[38] B. Kleihaus, J. Kunz and M. List, Phys. Rev. D **72**, 064002 (2005) [gr-qc/0505143].
[39] M. Gleiser and J. Thorarinson, Phys. Rev. D **73**, 065008 (2006).
[40] V. A. Gani, N. B. Konyukhova, S. V. Kurochkin, and V. A. Lensky, USSR Comput. Math. Math. Phys. **44**, 1968 (2007).
[41] N. Sakai and M. Sasaki, Prog. Theor. Phys. **119**, 929 (2008). T. Tamaki and N. Sakai, Phys. Rev. D **81**, 124041 (2010). N. Sakai, H. Ishihara and K.-I. Nakao, Phys. Rev. D **84**, 105022 (2011)
[42] M. I. Tsumagari, E. J. Copeland and P. M. Saffin, Phys. Rev. D **78**, 065021 (2008). E. J. Copeland and M. I. Tsumagari, Phys. Rev. D **80**, 025016 (2009).
[43] P. Bowcock, D. Foster and P. Sutcliffe, J. Phys. A **42**, 085403 (2009).
[44] H. Arodz and J. Lis, Phys. Rev. D **77**, 107702 (2008); Phys. Rev. D **79**, 045002 (2009).
[45] G. Gabadadze and R. A. Rosen, Phys. Lett. B **666**, 277 (2008).
[46] L. Campanelli and M. Ruggieri, Phys. Rev. D **80**, 036006

(2009).

[47] M. Mai and P. Schweitzer, forthcoming.

[48] M. von Laue, Ann. Phys. (Leipzig) 340, 524 (1911). I. Białynicki-Birula, Phys. Lett. A **182**, 346 (1993)

[49] R. Rajamaran, Solitons and Instantons (North-Holland, Amsterdam, 1982).

[50] Thomas Young, Phil. Trans. R. Soc. Lond. **95**, 65 (1805). Pierre-Simon Laplace, "Mécanique céleste" (1806). For a review and pedagogical derivations see: J. Pellicer, V. García-Morales, and M. J. Hernández, Phys. Educ. 35, 126 (2000).

[51] N. Graham, Phys. Lett. B **513**, 112 (2001).

[52] F. Ellinghaus [HERMES Collaboration], Nucl. Phys. A **711**, 171 (2002).

[53] A. V. Belitsky, D. Müller and A. Kirchner, Nucl. Phys. B **629**, 323 (2002). A. V. Belitsky and D. Müller, Nucl. Phys. A **711**, 118 (2002).

[54] CLAS Collaboration, "Jefferson Lab PAC 39 Proposal Timelike Compton Scattering and J/ψ photoproduction on the proton in e^+e^- pair production with CLAS12 at 11 GeV," (2012).